GFD Lecture 7: Ice-Ocean Interactions around Antarctica

Adrian Jenkins; notes by Federico Fuentes and Madelaine Gamble Rosevear

June 27, 2017

This document comprises the third review lecture given by Adrian Jenkins during the 2017 Geophysical Fluid Dynamics program at the Woods Hole Oceanographic Institution (WHOI). It is about the ice-ocean interaction in the continent of Antarctica, and is divided in two parts: cold water regimes and warm water regimes. Several figures and figure captions were copied literally or almost literally from their original sources to facilitate comprehension. In those cases, the relevant references are given.

1 Cold Water Regimes

1.1 Surface properties of Antarctica

For ease of reference, a map of Antarctica is included (Figure 1).

Figure 1: Map of Antarctica (image from NASA is in the public domain).

The continent of Antarctica is uniformly surrounded by very cold near-freezing water close to the surface. However, the distribution of near-surface (0-100 m) salinity is not as simple. Indeed, it can vary depending on precipitation and redistribution by sea ice, which adds salt during formation and fresh water when it melts. This can be observed in Figure 2, where the ocean tends to be fresher towards the north. Wherever the salinity is higher, it is easier to deepen the cold layer of water.

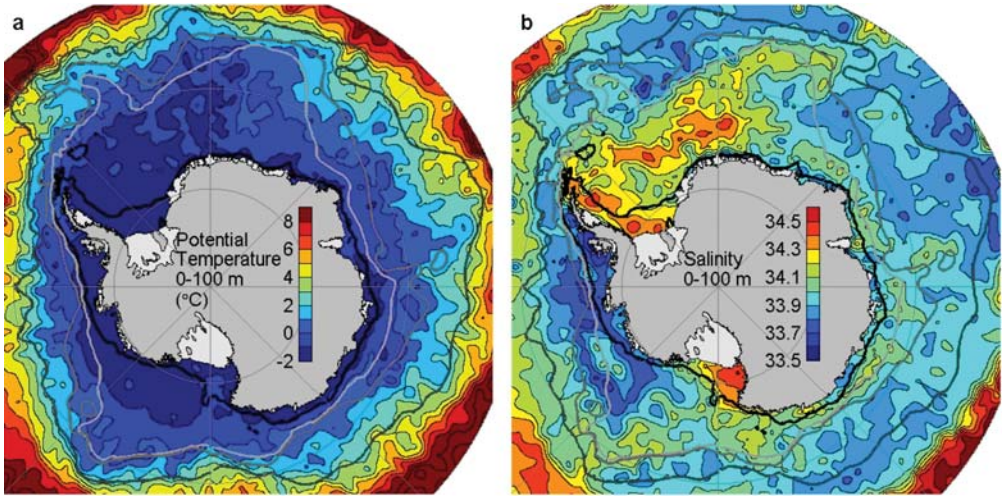

Figure 2: Near-surface temperature and near-surface salinity in the continent of Antarctica.

Around the Antarctic peninsula precipitation is high because the westerlies (winds blowing from west towards east, i.e., clockwise in Antarctic maps) encounter steep topography on the Antarctic Peninsula and are forced to rise, losing moisture as snowfall. This orographic effect can be observed in Figure 3, which shows the surface mass balance (effectively the snowfall) on the continent. The precipitation is then much lower in the Ross and Weddell seas due to the cold dry air which flows from the interior of the continent. Freezing (ice production) occurs pretty uniformly around the continent.

Strong katabatic winds (from higher elevations to lower elevations) are carried by the high and steep topography, especially in East Antarctica, where winds with speeds up to 320 km/hr have been reported in winter. These katabatic winds feed the near-coastal easterly winds. Meanwhile, in the Ross and Weddell seas winds are deviated north by topographic barriers. All this can be observed in Figure 4.

1.2 Shelf properties of Antarctica

In [23] an idealised model was used to study the processes setting the shelf water properties. The transport of relatively warm and salty circumpolar deep water (CDW) across the Antarctic slope front (ASF) (which almost completely surrounds the Antarctic continental shelf) was of particular interest, as the steep isopycnals (surfaces of constant density) associated with the ASF provide a barrier to on-shelf transport. The model was idealized by being essentially 2D, with no variations in the along-shore direction and periodic boundary conditions assumed. This is shown in Figure 5.

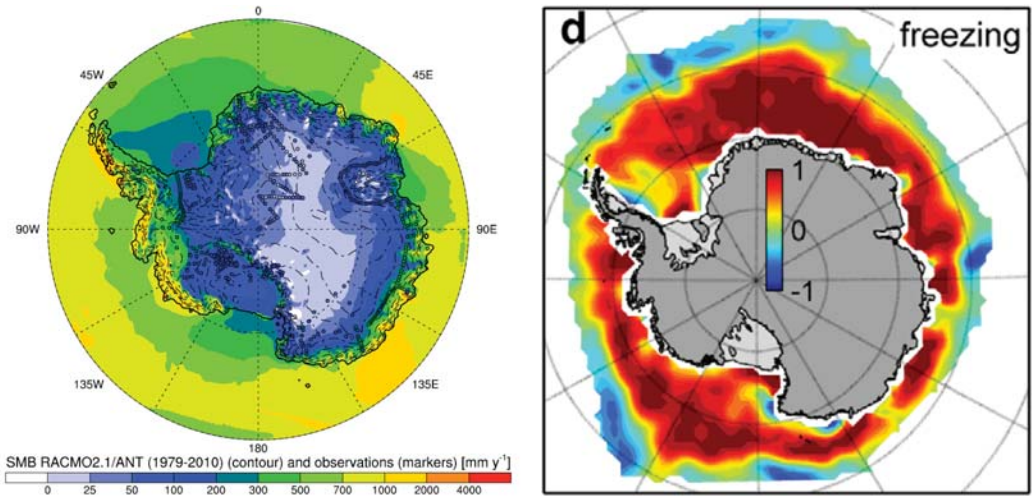

Figure 3: *Left:* Mean (1979-2010) surface mass balance (SMB) in mm w.e./yr (where w.e. means water equivalent) using simulations and observations. Note that on the seasonal sea-ice, SMB equals precipitation (P) minus surface sublimation (SU_s) and on open ocean $SMB = P$ [13]. *Right:* Mean concentration difference from residual freezing (does not represent ice *thickness*!) [5].

The investigation showed that shelf-water properties were mainly defined by wind-driven transport of Antarctic surface water (AASW) and by mesoscale eddies carrying CDW along isopycnals. Weaker winds allowed more warm CDW to flow onto the shelf, heating up the shelf waters, as did broader and deeper shelves. A higher surface salt flux (representative of higher sea ice formation) had the same effect, as it increased the production and outflow of cold, salty Antarctic bottom water (AABW). It is the presence of AABW that creates a connection between the shelf waters and the offshore CDW and allows mesoscale eddies to transport CDW onto the shelf. All these results are shown in Figure 6.

Another process that affects the shelf water properties is precipitation. When precipitation is high, the upper ocean is stabilised and the thermocline is shallower, thus in regions with high precipitation and weak coastal easterly winds (i.e. the Antarctic peninsula), warm CDW intrudes onto the shelf. Meanwhile, in regions where precipitation is lower and coastal easterlies are stronger, downwelling (accumulation and sinking of higher density water below lower density water) is sufficient to exclude CDW from the shelf. In the case where precipitation is low and the sea ice production is high, cold, salty shelf water is present.

This picture is confirmed by comparing temperature and salinity (Figure 7), precipitation (Figure 3) and winds (Figure 4) with shelf properties observed around Antarctica (Figure 8). At depth, the shelves are dominated by cold and salty shelf water off the coasts of the Filchner and Ross ice shelves; by cold and fresh AASW off the coasts of Dronning Maud Land and Wilkes Land; and by warm and salty CDW off the coast of Ellsworth Land and the Antarctic peninsula (see Figure 1 for geographic references).

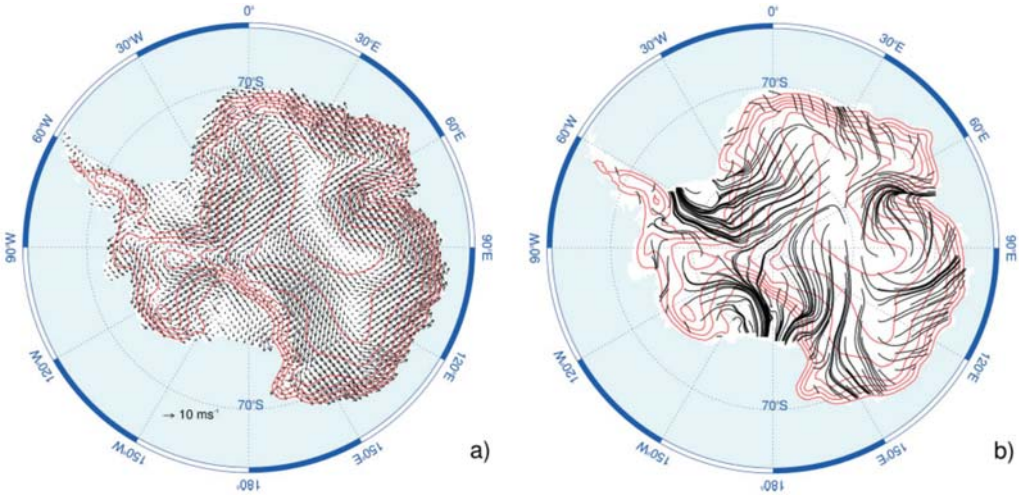

Figure 4: *Left:* Mean winter wind vector. *Right:* Mean winter stream lines. Data is from 1980-93. The elevation of the surface is shown by contour lines in red [24].

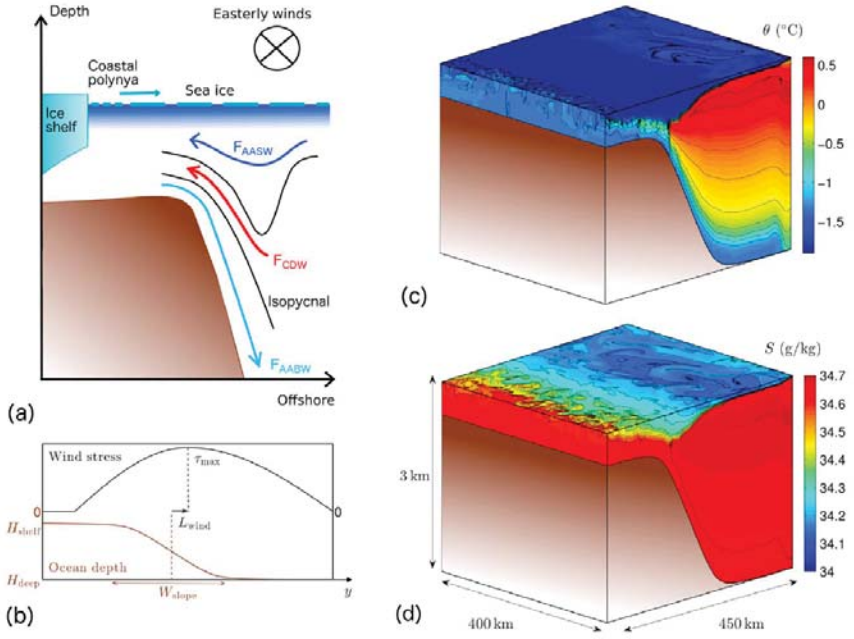

Figure 5: Taken from [23]. (a) Schematic cross-section of the Antarctic slope front (ASF), which separates the continental shelf waters from the warm circumpolar deep water (CDW) at mid-depth offshore. In regions of Antarctic bottom water (AABW) outflow, such as the western Weddell and Ross Seas, isopycnal (i.e. constant density) surfaces connecting the shelf waters to CDW may facilitate onshore heat transport and AABW export via the action of mesoscale eddies. (b) Schematic profiles of ocean depth, along-shore surface wind stress, and associated parameters. (c) potential temperature profile used as reference, where eddy boluses of warm CDW are visible crossing the shelf break. (d) Salinity profile used as reference.

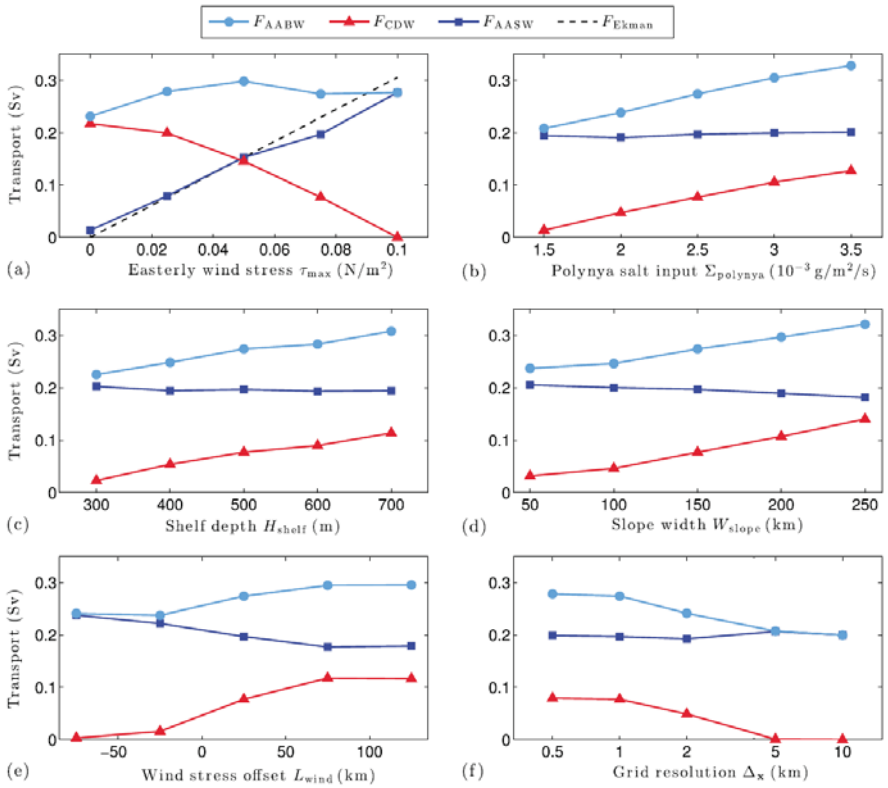

Figure 6: Taken from [23]. *Left:* Sensitivity of the transports crossing the Antarctic slope front (ASF) of Antarctic surface water (F_{AASW}), circumpolar deep water (F_{CDW}), and Antarctic bottom water (F_{AABW}). The sensitivity is to (a) the wind stress maximum amplitude $\tau_{\max}$, (b) the brine rejection rate on the continental shelf Σ_{polynya}, (c) the depth of the continental shelf H_{shelf}, (d) the width of the continental slope W_{slope}, (e) the offset of the wind stress maximum from the center of the continental slope (L_{wind}), and (f) the model's horizontal grid spacing Δ_x. In (a) the theoretical wind-driven southward surface Ekman transport is also shown, and it agrees closely with the shoreward transport of Antarctic surface water (AASW).

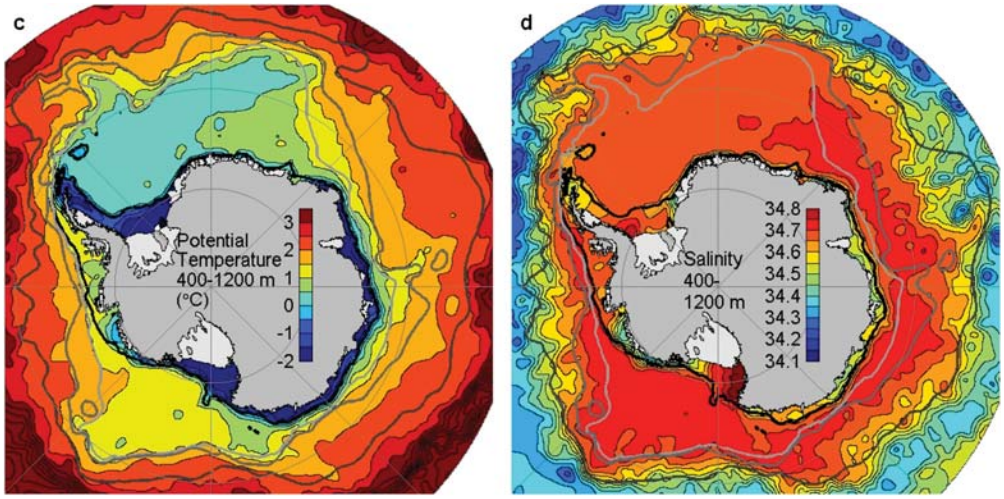

Figure 7: Deep water temperature and salinity in the continent of Antarctica.

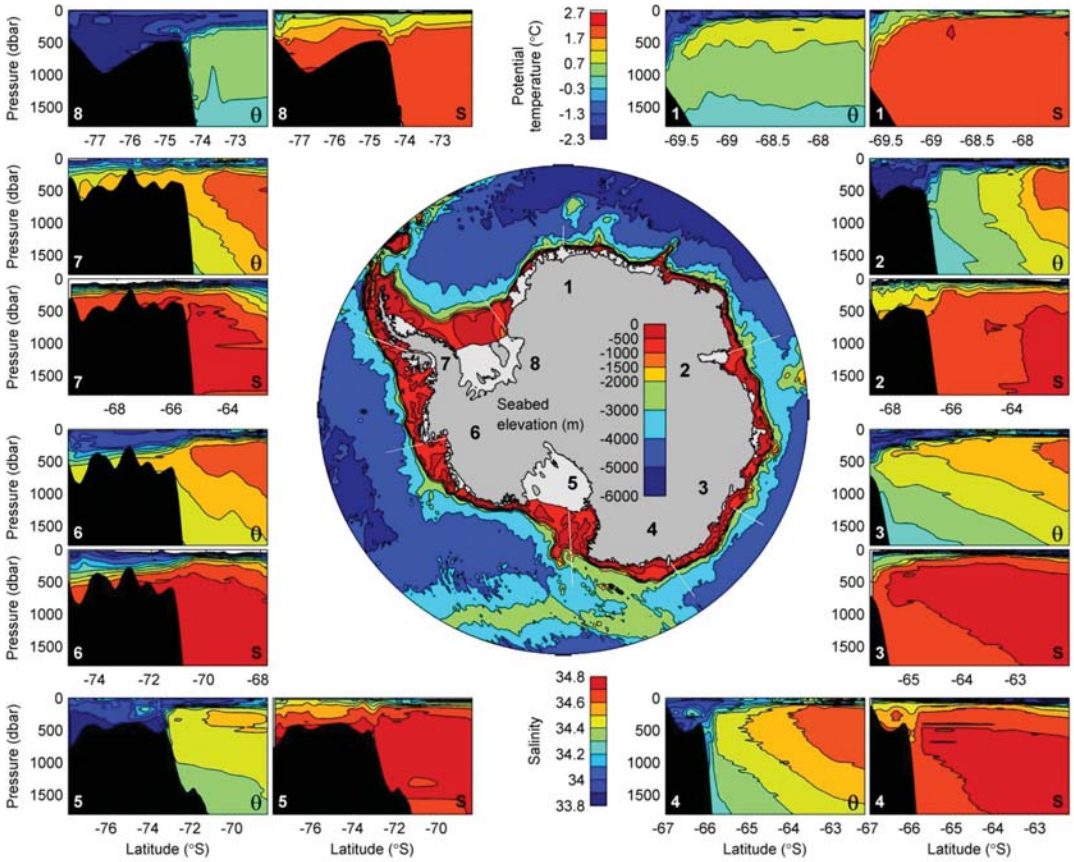

Figure 8: Temperature (θ) and salinity (S) profiles at different parts of Antarctica. At depth the shelves are dominated by either: cold and salty shelf water (8, 5, and to a lesser extent 2 and 4); cold and fresh Antarctic surface water (AASW) (1, 3, and much of the area around 2 and 4); or warm and salty circumpolar deep water (CDW) (7 and 6).

1.3 Melting modes

The different melting modes are illustrated in Figure 9, and are briefly described next:

- Mode 1: This form of melting occurs when shelf water (SW) dominates. There are extensive areas of refreezing and melt rates on the order of 0.1 m/yr. Both SW and ice shelf water (ISW) are sufficiently dense to form Antarctic bottom water (AABW).
- Mode 2: Here, the warmer circumpolar deep water (CDW) dominates. There is no refreezing and much higher melt rates on the order of 1-10 m/yr are observed.
- Mode 3: This occurs when Antarctic surface water (AASW) dominates and CDW intrusions only occur at the seabed. Some refreezing does occur and due to AASW being seasonally warmer than SW, higher melt rates than Mode 1 are observed; on the order of 0.1-1 m/yr.

1.4 Melting mode 1

In the southern Weddell Sea, where the Filchner-Ronne ice shelf (FRIS) lies, the cold SW is dominant and denser than CDW. The complicated seabed and ice shelf geometry results in a modified (with respect to the usual) pattern of melting and freezing, as shown in Figure 10, where the basic "ice pump" mechanism is visible from the satellite data. From the figure it can be observed that relatively little warm water enters the cavity, and that the highest melting occurs at depth, near the grounding line.

Figure 11 presents results from models, which show an overturning circulation, but also strong horizontal flows guided by ice-base and seabed topography. The presence of tides induces much stronger circulation, where increased melting results in higher buoyancy forcing. The model also reproduces the observed pattern of melting where the warm water enters the cavity and reaches the deep grounding lines, while freezing is present along the outflow paths (right in Figure 11). The freezing and melting are low when the effects of the tides are not considered, but increase significantly with tidal forcing. Even though tides generate only weak time-averaged currents, tidal currents can dominate the instantaneous flow if the buoyancy forcing is weak. In that case, the tides control the turbulent transport of heat to the ice shelf base.

The outflows of ice shelf water (ISW) are possibly supercooled, due to the fact that inflowing waters have a temperature close to the surface freezing point. The addition of meltwater at depth, where the *in situ* freezing temperature is even lower due to the effect of pressure, means that the buoyant outflow may become supercooled as it rises. In that case, platelet ice may form and can generate regions of very thick (about 10 m) land-fast sea ice. These insights can be appreciated in Figure 10 (bottom).

Most ISW exits the cavity at depth and contributes to the Antarctic bottom water (AABW) formation as it spills off the continental shelf. Similar processes occur in the Ross Sea, but melting and production of ISW appear to be slightly lower, probably because the ice shelf is thinner on average.

Ice shelves of the Ross and Weddell seas are probably relatively insensitive to climate change. The shelf water will be fixed at the surface freezing point as long as enough sea ice

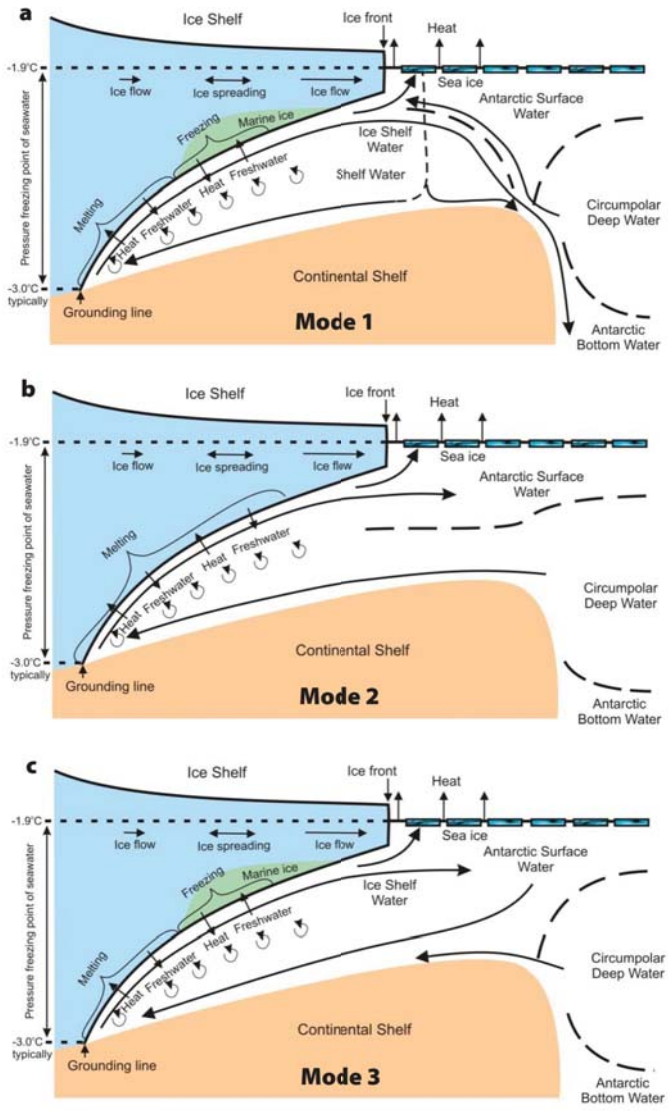

Figure 9: Taken from [8]: Three modes of sub-ice-shelf circulation and associated stratification on the continental shelf. (a) In Mode 1, dense shelf water (SW), formed by brine rejection beneath growing sea ice, dominates the sub-ice cavity. SW has a temperature at or close to the surface freezing point, and can melt ice at depth only because of the pressure dependence of the freezing point. Some refreezing occurs in the cavity because the water produced by melting (ice shelf water (ISW)) becomes supercooled as it rises along the shoaling ice shelf base. (b) Mode 2 dominates if SW is absent and circumpolar deep water (CDW) is the densest water on the shelf. CDW temperatures are typically around 3°C above the surface freezing point so melting is rapid, no ISW forms, and there is no refreezing. (c) Mode 3 dominates where both SW and CDW are absent, leaving Antarctic surface water (AASW) as the densest water on the shelf. Only the upper layer of AASW is seasonally warmer than the surface freezing point, so melt rates are low and ISW formation and refreezing can result. Although the CDW is denser, its access to the shelf is limited by the deepening of the AASW layer at the coast, where the southward Ekman transport driven by the easterly wind is blocked. Note that in (a), Modes 2 and 3 may influence the outer cavity because AASW and modified CDW are present in the upper water column, while in (b), Mode 3 melting may occur above the permanent thermocline separating AASW and CDW.

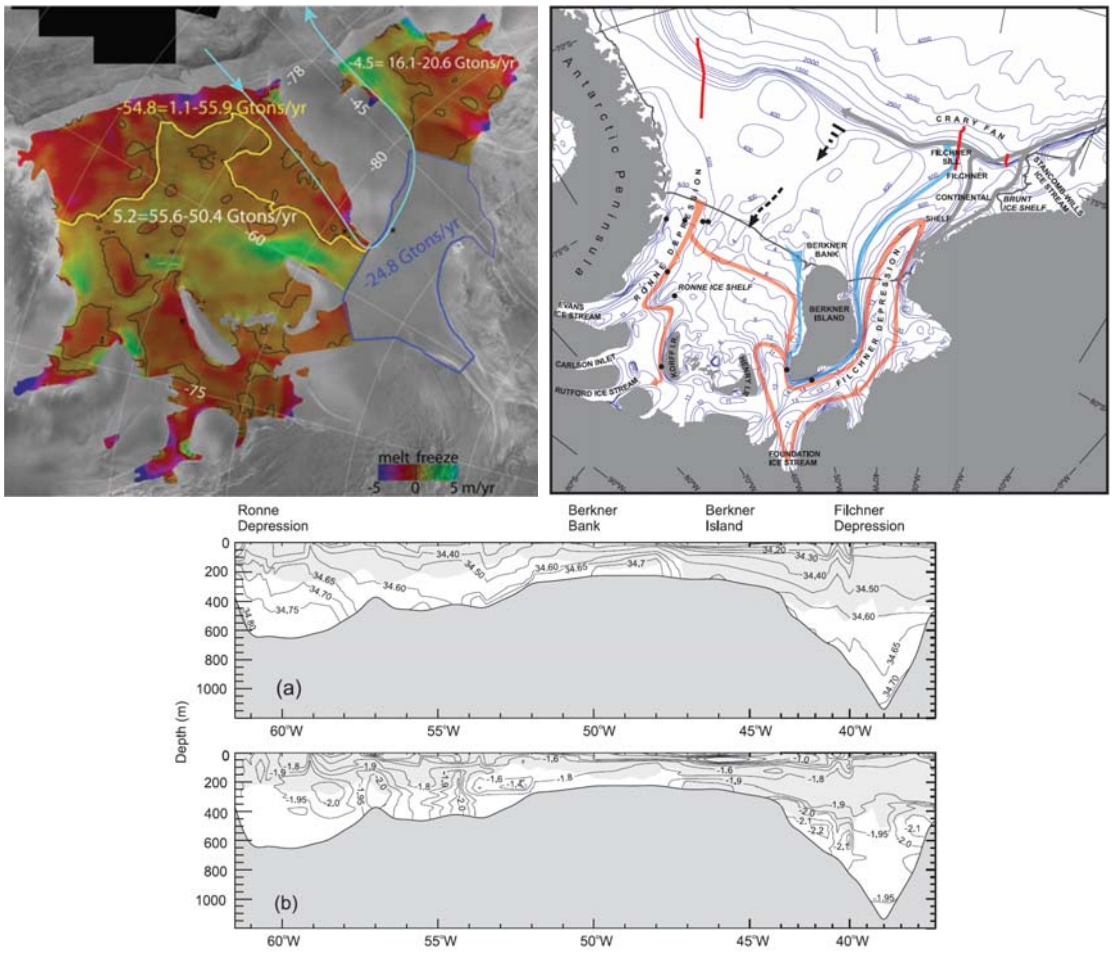

Figure 10: *Top left:* Basal melt rates under assumptions of steady-state ice shelf and conservation of mass. Positive values represent freezing and negative values melting (with color saturation for magnitudes over 5 m/yr). Yellow line shows separation of region with strong melt at the Ronne shelf, while light blue lines illustrate inferred ocean circulation paths [10]. *Top right:* Southwestern Weddell Sea. Bathymetric contours are labeled in hundreds of meters beneath the ice shelves. Dotted black arrows indicate inflow of modified warm deep water (MWDW) [18]. *Bottom:* (a) Salinity and (b) potential temperature at the Filchner and Ronne ice fronts, where the light gray represents the draft of the ice shelf in the ice front [18].

is produced. One model suggests the possibility of a future regime change [4]. It argues that thinning of sea ice may increase the wind stress and strengthen the inflow of modified CDW. However, as this happens, there must also be a decrease in shelf water density.

1.5 Melting mode 3

The Fimbul ice shelf (FIS) is located in the eastern Weddell Sea, where wind-forced downwelling of Antarctic surface water (AASW) dominates and keeps the shelf cold. Note that the topography in this region is very steep, as can be observed in Figure 12. It is thought that the wind-forced overturning is opposed by eddy overturning of the front, which brings warm water on-shelf at depth (see Figure 12). This has a subtle difference to the case

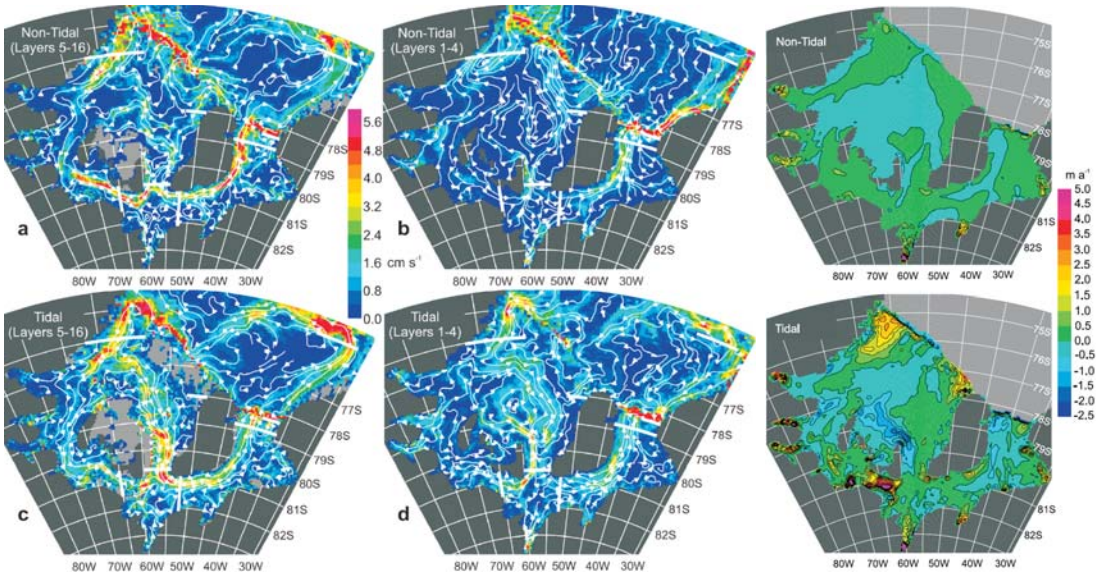

Figure 11: From [14]. *Left-center:* Flow lines of the modeled mean annual circulation in (a) the lower twelve layers without tides, (b) the upper four layers (including the mixed layer) without tides, (c) the lower twelve layers with tides, and (d) the upper four layers with tides. The color scale shows the mean current speed. *Right:* Mean basal ice melt rates beneath the Filchner-Ronne ice shelf (FRIS) in cm/yr from the model for non-tidal (top) and tidal (bottom) simulations. Negative values indicate freezing.

where shelf water (SW) formation creates an isopycnal connection to the deep waters off-shelf. That being said, an analogous model with the ice shelf included and without any SW formation, shows a similar result. As observed in Figure 12 (right), a weaker easterly wind allows warmer CDW to intrude along the seabed (note the higher temperatures at the seabed when the wind is 3 m/s as compared to when the wind is 9 m/s). Therefore, the wind is a fundamental factor of the heat transfer.

In the summer, the seasonally warmer upper layer of Antarctic surface water (AASW) drives melting in the outer cavity (see left of Figure 13). This layer is relatively fresh and typically too thin to get beneath the ice, but again, wind-forced coastal downwelling is what allows it to access the Fimbul cavity. However, in this case, stronger easterly winds lead to a greater flux of warm water into the cavity.

Before observations were made in the Fimbul cavity, a modeling study suggested that more circumpolar deep water (CDW) could be present at depth (see right of Figure 13). This ended up being wrong, but for an interesting reason. An eastward-flowing undercurrent beneath the westward-flowing AASW carried CDW along the upper slope. It turned on-shelf within a seabed trough that cut the shelf edge and carried CDW beneath the ice shelf. Stronger easterly winds could exclude the inflow by pushing the front and the undercurrent deeper. This undercurrent has been identified in observations, but always deep down on the continental slope [1].

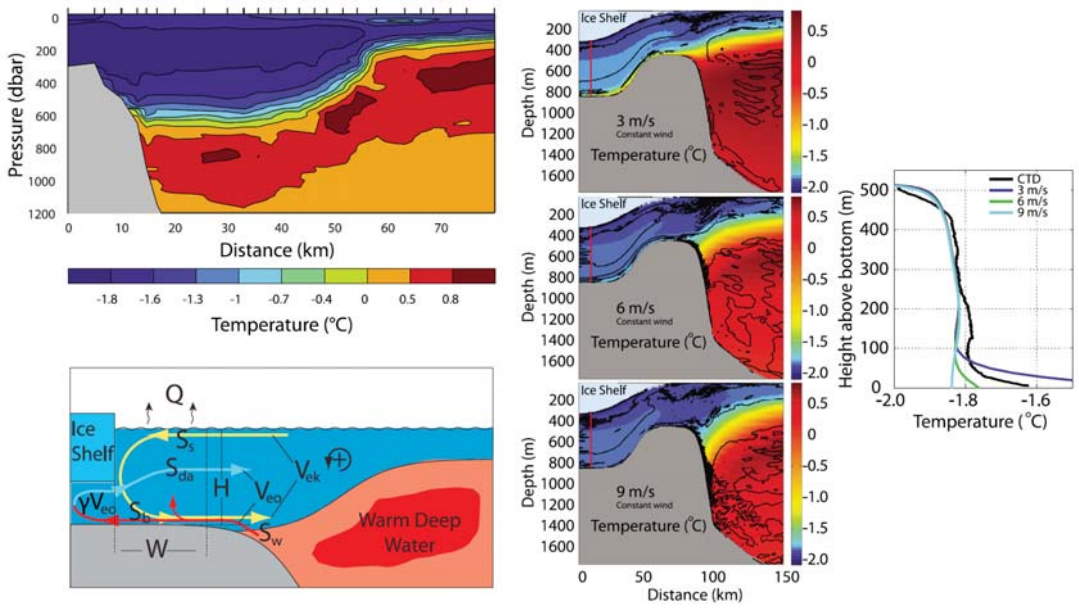

Figure 12: From [19]. *Top left:* Temperature section across the Antarctic slope front (ASF) at 17°W showing the typical structure of the ASF. *Bottom left:* Sketch illustrating the hypothesized exchange processes across the ASF. Yellow arrows illustrate Ekman overturning (V_{ek}), while red and blue arrows illustrate the overturning of the slope front (V_{eo}) and the sub-ice shelf overturning (γV_{eo}) respectively. *Right:* The along-slope-averaged temperature estimated from daily snapshots. Negative velocities are to left. The black lines are contours of zero residual velocity. Further right is the observed temperature profile beneath the Fimbul ice shelf (FIS) (in black) along with the modeled temperature profiles (in colors) taken from the vertical red line in the previous plots.

1.6 A note on the warm water regimes

Warm derivatives of warm circumpolar deep water (CDW) are found at depth on the shelf from 55-155°W. Often, it is assumed that the dominant processes are common and connected with the proximity of the Antarctic circumpolar current (ACC). Nevertheless, the ACC does not reach the continental slope until about 90°W (see left of Figure 14). In the Amundsen Sea it flows north of the Marie-Byrd Seamounts.

In the Bellingshausen Sea, upper CDW comes on the shelf as eddies that shed from the ACC (see right of Figure 14). Thus, upper CDW is not confined to troughs. On the other hand, lower CDW intrusions follow the trough topography and appear to be steadier. Meanwhile, in the Amundsen Sea, the deeper thermocline seems to exclude most upper CDW, while lower CDW intrudes along the troughs. The presence of CDW on the shelf is not a novelty, since it was observed as early as the Belgian Antarctic expedition from 1897-1899.

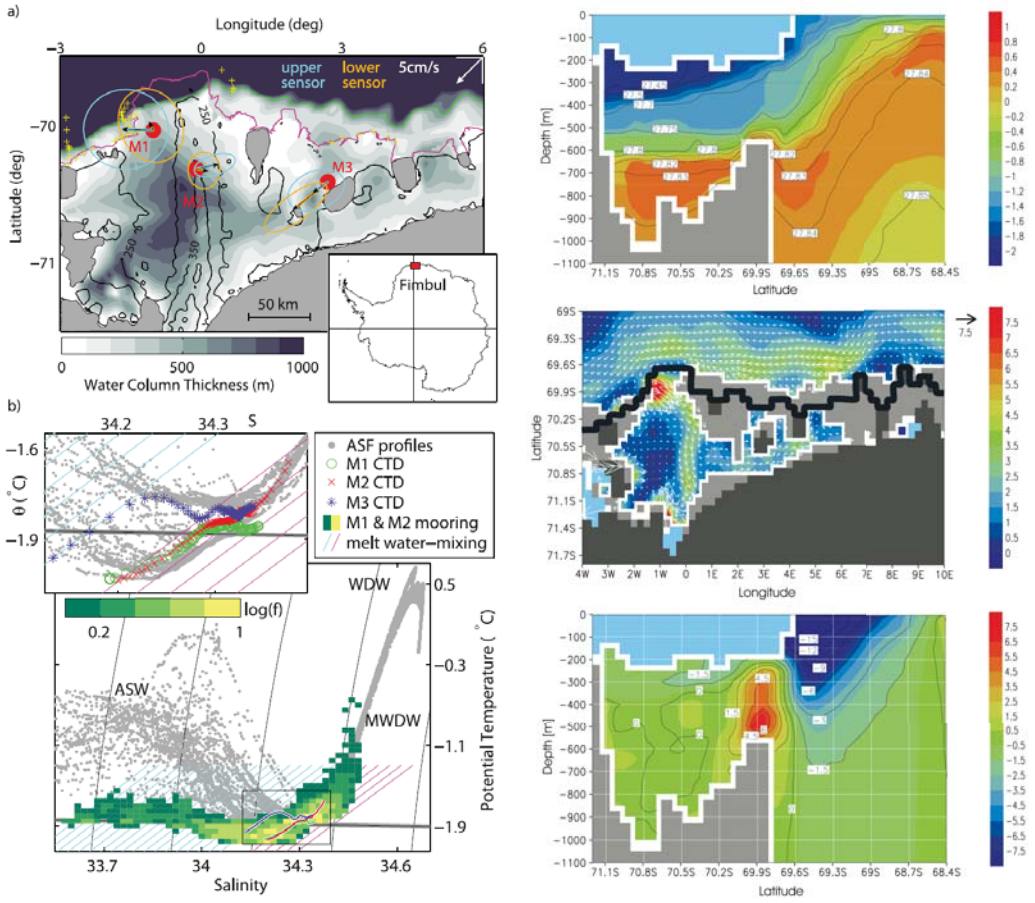

Figure 13: *Left:* From [3]. (a) Map of Fimbul ice shelf (FIS), with mooring locations M1, M2, and M3 indicated by red dots, together with water column thickness (gray shading). Black contours show the ice draft in 100 m intervals. The ice front is shown in magenta, and the continental shelf break in green (1500 m isobath). Vectors originating at each site show the annual mean value of the currents, surrounded by their associated variance ellipses (the white arrow in the upper right corner indicates the velocity scale). (b) Potential temperature-salinity diagram comparing observations below the FIS with coastal hydrography. The color shading shows the relative occurrence of different water masses at the mooring sensors, binned in T-S space, with yellow indicating many observations on a logarithmic scale. Two arrays of melt water mixing lines, as described in the text, highlight the melting regimes associated with Antarctic surface water (AASW or ASW) (blue) and modified warm deep water (MWDW) (magenta). *Right:* From [21]. (Top) Annual mean potential temperature (°C) along 1°W in the steady state solution. FIS is shown in light blue, and the bedrock in gray. Potential density contours are shown as black lines. (Middle) Annual mean flow at 450 m depth in the steady state solution. The color scale shows current magnitude (cm/s) and the arrows are current vectors with a 7.5 cm/s arrow to scale in the upper right corner. The thick black line is the ice front of FIS. (Bottom) Annual mean eastward current speed (cm/s) at 1°W in the steady state solution.

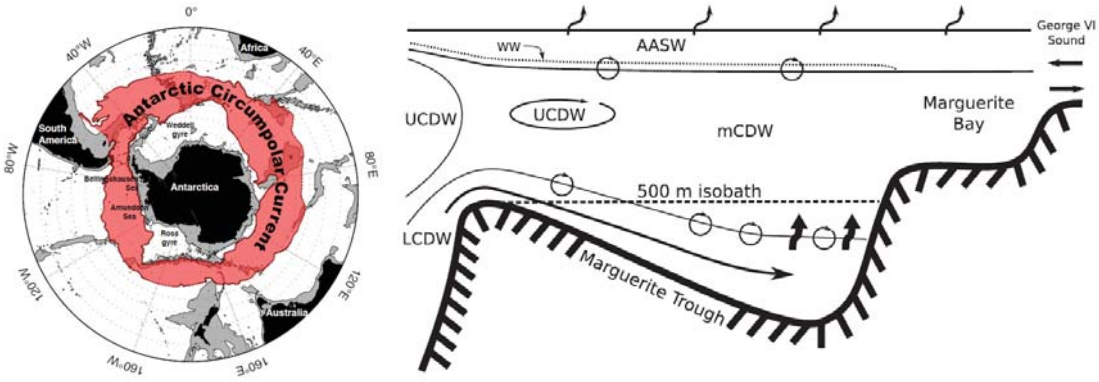

Figure 14: *Left:* From [15]. Location of climatological Antarctic circumpolar current (ACC), transporting warm upper circumpolar deep water (UCDW). The ACC flows along the slope-shelf break for the entire western Antarctic. Bathymetry shallower than 3 km is shaded. *Right:* From [16]. Conceptual diagram showing the characteristics of circumpolar deep water (CDW) intrusions to the western Antarctic Peninsula (wAP) shelf. UCDW intrudes on the shelf in the form of relatively small and frequent middepth features. Lower circumpolar deep water (LCDW) is found at the bottom of deep depressions. The thick black arrows represent upwelling of LCDW water to the overlying water, and the rounded arrows represent mixing across layers.

2 Warm Water Regimes

Here, we turn our attention the high melt regime driven by the transport of warm circumpolar deep water (CDW) onto the continental shelf, or mode 2 melting. Whilst CDW is present all around Antarctica, there are only a few regions in which it can penetrate beneath ice shelves. The Amundsen sea sector is one such region.

2.1 Mean state

In the eastern Amundsen Sea, the broad continental shelf is interspersed with a series of deeper troughs (Figure 15). These troughs, which were carved out by glaciers during previous advances of the Antarctic ice sheet, now provide a pathway for CDW to access the ice shelves in the region.

Moving east to west along the shelf, the thermocline deepens (Figure 16) and the CDW present below becomes cooler. In the west, the combination of a shallower shelf and a deeper thermocline means that CDW is almost completely blocked from coming on-shelf. As a result, the ice shelves in the western part of the Amundsen sector are close to a transition to the cold water regimes discussed in Part I, where the shelf is effectively isolated from CDW.

2.1.1 Observations of heat transport to Pine Island Glacier

Access for CDW to Pine Island Glacier occurs through two troughs, Pine Island Trough East (PITE) and Pine Island Trough West (PITW). Observations of PITW show an inflow of CDW of about 0.2 Sv which delivers an on-shelf heat flux of around 2.8 TW [25].

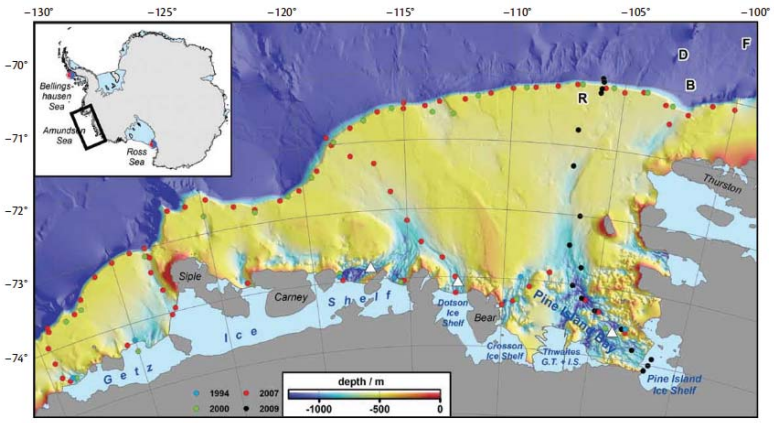

Figure 15: The Amundsen Sea continental shelf and floating ice shelves of the region. Figure taken from [6].

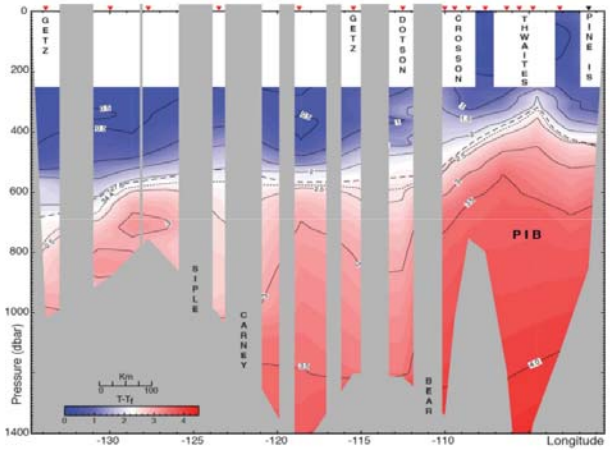

Figure 16: Temperature (°C) above pressure freezing point ($T - T_f$) moving along the shelf, with nominal ice shelf draft (white). Figure from [6]

Along shelf flow is dominated by the Antarctic Slope Current, an eastward flow driven by winds off the Antarctic continent. Intriguingly, observations on the western side of PITW show a strong, eastward flowing undercurrent carrying CDW along the shelf edge (see upper two panels of Figure 17). The troughs are approximately 30 km wide, considerably larger in scale than the Rossby radius of deformation which is on the order of 3 km, so when the current encounters the trough it is steered south onto the shelf (see lower two panels of Figure 17).

Kimura *et al.* (in review) find that the inflows combined supply about 6 TW of heat to the shelf. Of this heat, approximately one third is lost to the atmosphere, one third is used to melt ice shelves and one third is carried westward by the on-shelf circulation.

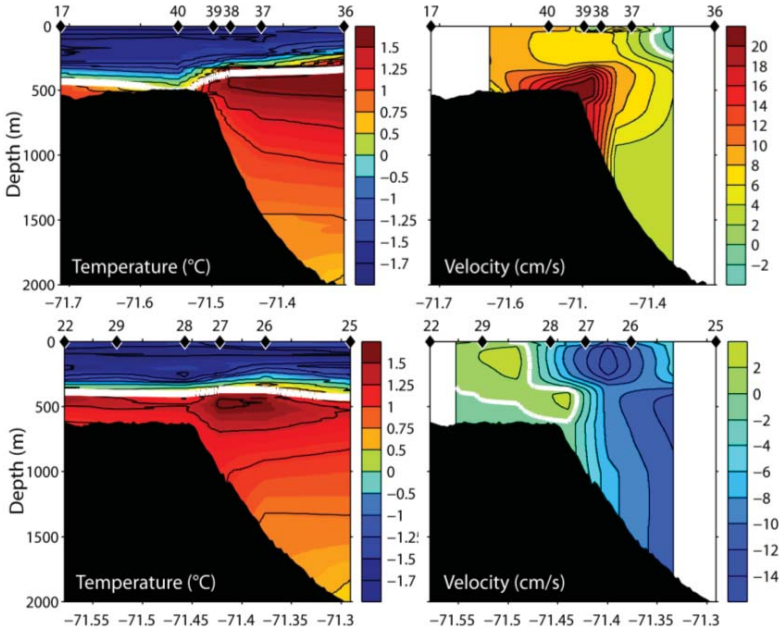

Figure 17: Potential temperature and geostrophic velocity sections for two separate transects; one slightly westward of Pine Island Trough West (PITW) and the other at the entrance to PITW. Positive values are eastward flowing currents. Figure from [26].

2.2 Variability

2.2.1 Instrumental record

Conditions in the Amundsen Sea lie somewhere in between the strongly stratified conditions to the east (e.g. Marguerite Bay) and the weakly stratified conditions in the Ross Sea to the west. In Marguerite Bay the thermocline is extremely shallow and warm CDW occupies most of the water column (Figure 18), however the Ross Sea is almost uniformly cold with some freshening at the surface.

The thermocline depth in the Amundsen sea is highly variable and is sensitive to both wind and buoyancy forcing. Furthermore, variability in thermocline depth drives variability in ice shelf melt. Observations from in front of the Pine Island Glacier (PIG) calving front show that changes in the depth of the thermocline are accompanied by changes in meltwater fraction and thus ice shelf melt (Figure 19). At the PIG calving front, meltwater is identified as a warm, salty anomaly. This result, which is somewhat counter-intuitive as melting is associated with cooling and freshening, can be understood in terms of the watermasses in Figure 20. If the cavity beneath an ice shelf has the temperature-salinity (TS) properties of Ambient 1, warm, salty CDW (x_1) may drive melt and follow the meltwater mixing line to x_2. The mix of meltwater and ambient fluid will then rise in the water column to its level of neutral buoyancy. Tracing the isopycnal between x_2 and the open circle on Ambient 1, we can see that the meltwater mix will be warmer and saltier than the ambient fluid of the same density, and will therefore appear as a warm and salty anomaly. This effect will only occur if the slope of the ambient in TS space is steeper than the meltwater mixing lines; if

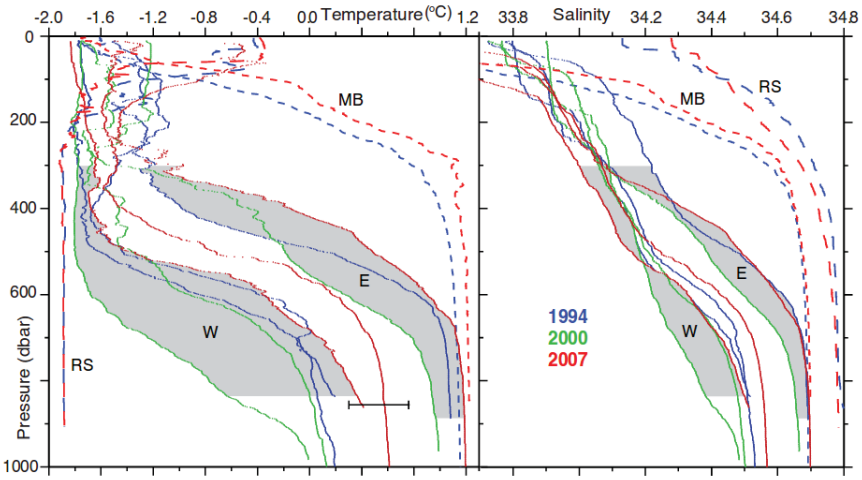

Figure 18: *In situ* temperature and salinity averages showing thermohaline properties in the Amundsen Sea for 1994, 2000 and 2007. Labels indicate profiles from east of Bear Island (E) and west of Siple Islands (W). The dashed profiles, which are provided for comparison, are from Marguerite Bay (MB) and near Ross Island (RS). Figure from [6].

the slope is shallower (e.g. Ambient 2) the water mass will be cooled and freshened through the addition of meltwater.

In the Amundsen sector, the ambient stratification is set by the mixing of Antarctic surface water (AASW) and CDW. Provided that the AASW salinity is above 33.6 psu, the CDW/meltwater mix will be warmer and saltier at any given density. In winter, the meltwater outflows contain enough heat to melt sea ice.

How different water masses interact with ice shelves is also determined by the geometry of the ice shelf cavity. Beneath Pine Island Glacier, a 300 m high seafloor ridge provides a partial barrier to inflowing CDW. Much like the relative depths of the thermocline and continental shelf control the flow of CDW onto the shelf, the relative positions of the thermocline depth to the ridge determine how much heat reaches the grounding zone. However, here a positive feedback may be present; the more the ice thins, the wider the gap over the ridge becomes, allowing more CDW to access the grounding line.

West of Pine Island Glacier, at the Dotson Ice Shelf, a time series of temperature sections across the calving front shows that variability in the depth of the thermocline is the primary influence on the average temperature of inflowing water, and that this drives extreme variability in melt fluxes. The melt fluxes calculated from oceanic properties are consistent with satellite-derived measurements of ice shelf melt rate.

Results from the Dotson suggest that melt rate is a non-linear function of temperature. Whilst it is difficult to ascertain this from the Dotson data alone, Figure 22 also includes an estimate of melt in cold water ice shelves, as we know that the pressure dependence of the freezing point allows melting to occur beneath an ice shelf even when the water masses driving it are at surface freezing point. Thus, the melt flux is positive definite even at zero degrees on Figure 22. As a result of this non-linearity, the Amundsen ice shelves are more sensitive to ocean variability because the mean state is warm.

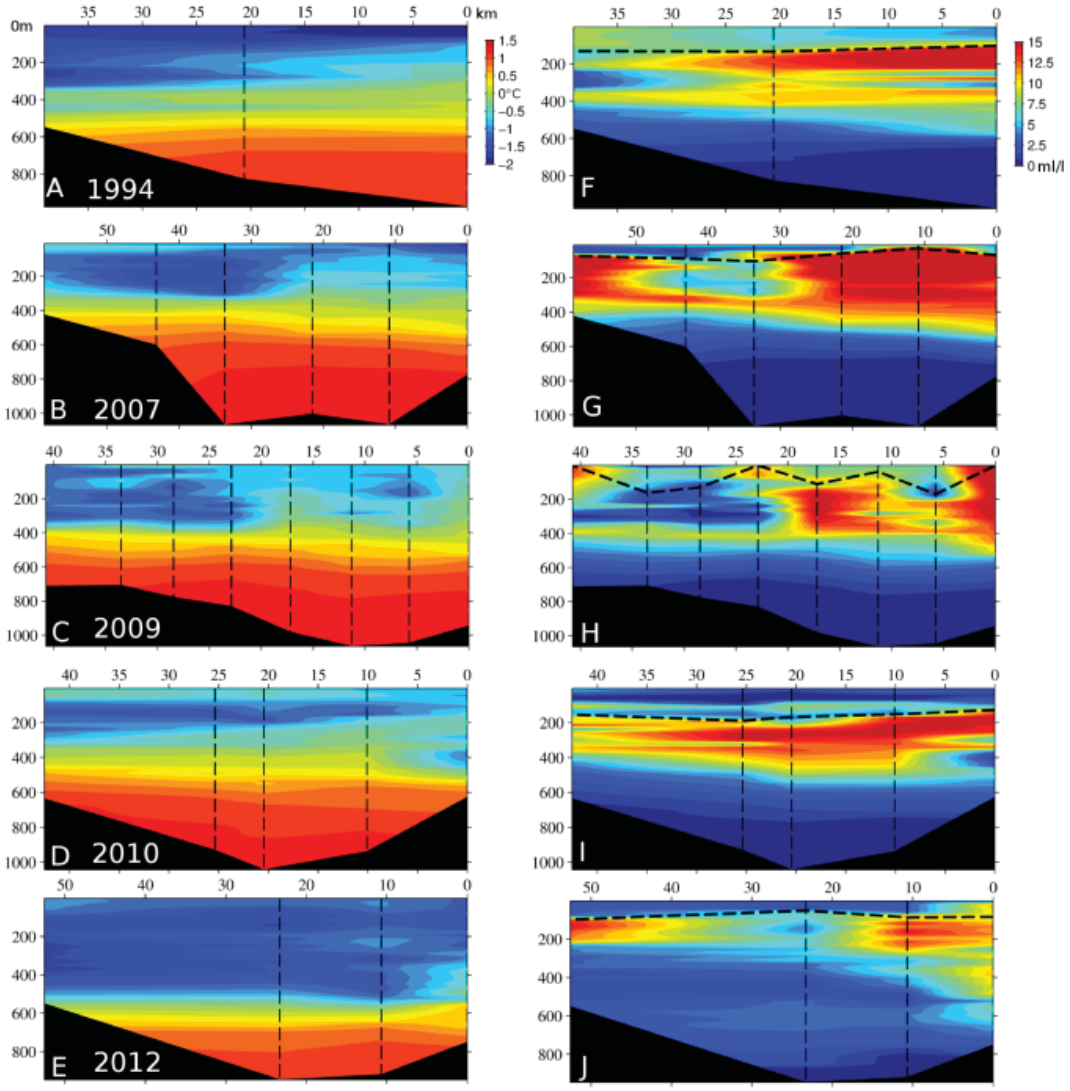

Figure 19: Potential temperature (A–E) and meltwater fraction (F–J) sections at the Pine Island Glacier ice shelf calving front for individual years of observation (labeled). Sections are facing into the cavity beneath the ice shelf. Figure from supplementary material of [2].

2.3 What's driving the variability?

Model results from Kimura *et al.* (in review) suggest that variability in shelf edge inflows rather than surface fluxes is the primary control on themocline depth, and hence on melt rates. Whilst surface fluxes affect the AASW layer, they have little impact at the depths that matter to the ice shelf.

The variability in the shelf edge currents themselves is driven by wind, although the mechanism for this is not yet clear. Periods of strong easterlies (Figure 23a) enhance downwelling on the shelf and buoyancy forcing in polynyas and suppress the slope front undercurrent, decreasing transport of CDW onto the shelf and making it more likely to mix with the overlying waters as it passes over the ridge. This results in an overall cooling and decrease in

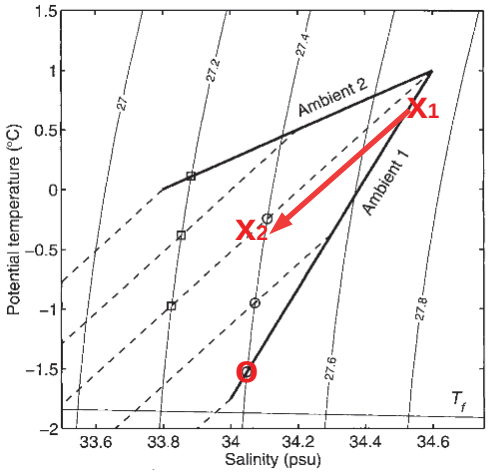

Figure 20: Potential temperature vs salinity diagram illustrating properties of two idealized ambient water columns (bold lines), with melt-water mixing lines (dashed lines) extending from the top, the bottom, and the midpoint of each. Open circles indicate possible properties produced by melting into Ambient 1, while open squares indicate the same for Ambient 2. Figure adapted from [7].

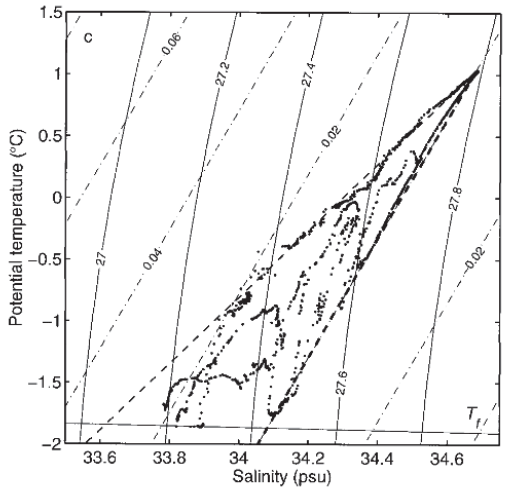

Figure 21: Potential temperature vs salinity plot at the calving front of Pine Island Glacier. Numbered solid lines are isopycnals, and the solid line near the bottom of the diagram indicates the surface freezing point. In (c) dashed lines represent approximations to the ambient trend in the main thermocline (bold) and a melt-water mixing line. The dash-dotted lines are contours of melt-water fraction. Figure from [7].

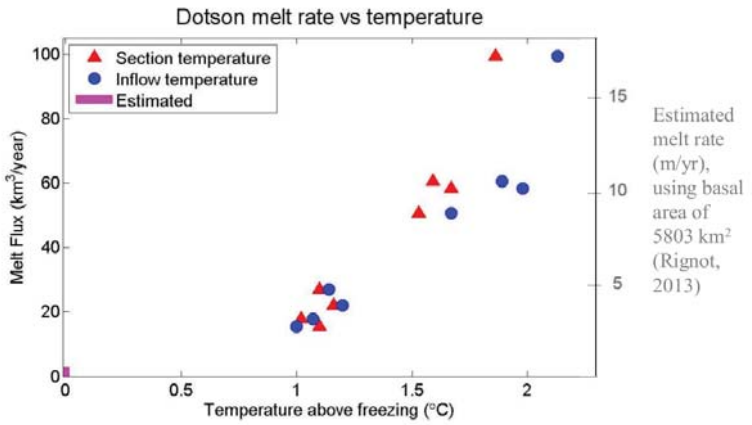

Figure 22: Average temperatures and melt fluxes from the Dotson Ice Shelf. Figure from Jenkins *et al.* (in preparation).

melt. Conversely, weaker easterly winds are often accompanied by weak westerlies at the shelf edge (Figure 23b). This enhances inflow of CDW which raises the thermocline, allowing more transport over the ridge and increased melting.

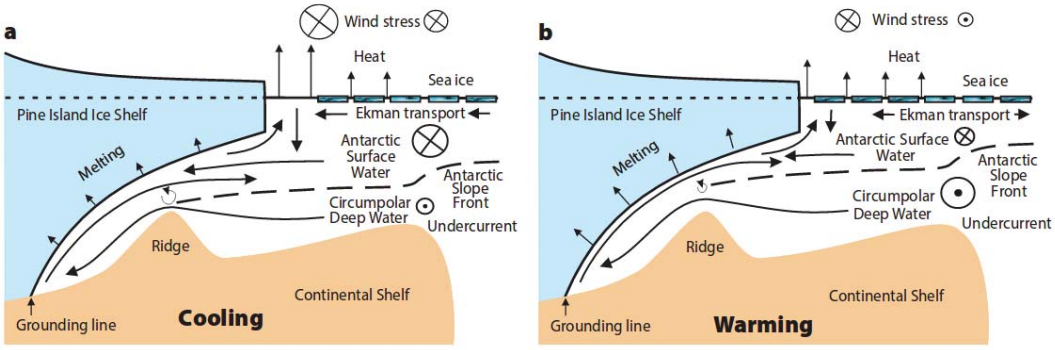

Figure 23: Schematic of processes that lead to (a) cooling and (b) warming of the eastern Amundsen Sea continental shelf. Figure from [9].

2.3.1 A mechanism for changing the winds

The weak easterlies in the Amundsen sector are themselves associated with El Niño Southern Oscillation (ENSO). Anomalous heating in the central equatorial Pacific triggers a standing Rossby wave that which results in sea level pressure anomalies in the Amundsen Sea. These anomalies weaken the easterly winds over the Amundsen Sea shelf and can result in westerly winds over the shelf edge.

Over the instrumental record, mooring and CTD (sonde used to measure conductivity, temperature and pressure) observations of inflow properties show a good agreement with zonal wind anomalies and central Pacific Sea Surface Temperature (SST) anomalies (Figure

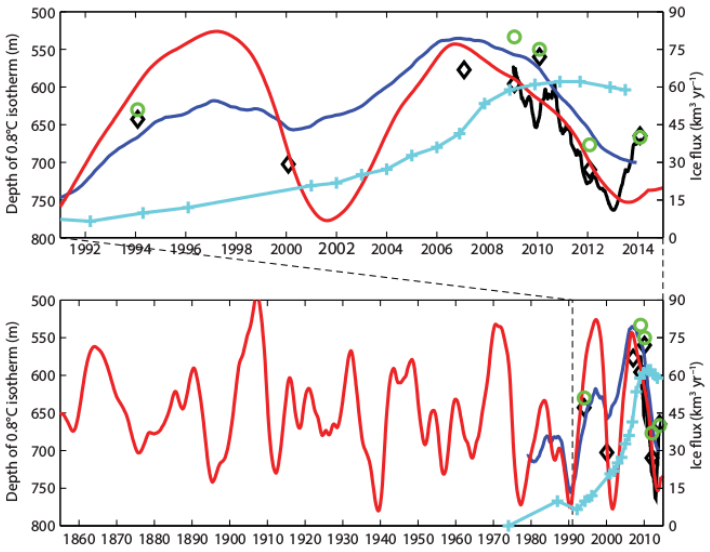

Figure 24: Proxies for thermocline depth on the inner shelf of the eastern Amundsen Sea (the upper panel is an expanded version over the observational period). The depth of the 0.8°C isotherm (left-hand axis) is extracted from mooring data (black line) and averages of summer CTD stations (black diamonds). Less direct proxies come from the cumulative zonal wind anomaly (dark blue line) and cumulative central tropical Pacific sea surface temperature anomaly (red line). Figure from [9].

24, upper panel), suggesting that the link between these may explain the dominant mode of variability.

2.4 Implications for driving ice sheet change

The Last Glacial Maximum (LGM) was the period during the last glacial cycle during which Earth's ice sheets were at their maximum extent. As such, the retreat of ice between the LGM and present day extent is used to understand the mechanisms for ice loss from Antarctica, and the speed at which they occur.

In the Amundsen sector, the retreat of ice from LGM to present day extent occurred mainly between 10 and 20 thousand years before present. In the following period, the margin appears to have been stable [12].

2.4.1 The retreat of Pine Island Glacier

Sediment cores from the ridge beneath Pine Island Glacier reveal that there has been recent change. Pre-1940s sediment records show only coarse grained sediments, transported by the glacier itself, to either side of the ridge (Figure 25). Behind the ridge is a small cavity of water, but this cavity has no connection to the ocean. Post 1945, the presence of fine grained sediments transported by plumes suggest the there was an oceanic cavity behind the ridge with a connection to the outer cavity, either through a bathymetric feature or due to tides. However, the coarse sediments on the front of the ridge demonstrate that the ice shelf is still pinned to the ridge. Post 1970, the presence of fine sediments on both sides of the ridge

suggest that this is when the cavity took on its current geometry. This assertion is confirmed by early satellite imagery.

Satellite radar interferometry since the early 1990s shows the glacier is still retreating, as are many others along the eastern Amundsen coastline.

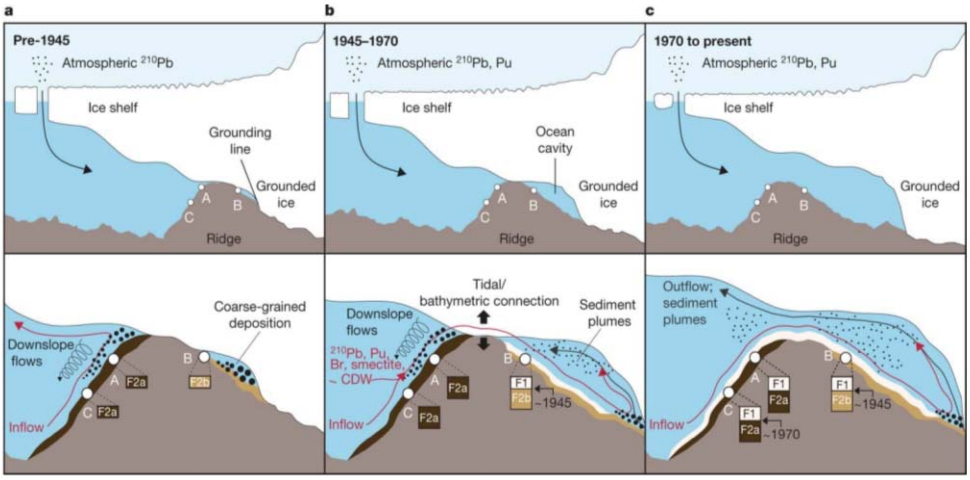

Figure 25: Sedimentation and processes beneath Pine Island Glacier. Figure from [22].

The retreat has been explained as a result of warming of the waters on the Amundsen Sea Shelf [20]. However, the study that published this result uses data up to early 2010, and thus does not include the subsequent cooling of shelf waters. Instead, the recent record of grounding line movement is more consistent with the ocean variability. Grounding line retreat has slowed during the cool phase and the Kohler Glacier has even re-advanced.

2.4.2 Glacier thinning

Analysis from satellite altimetry shows that the thinning of glaciers is not a continuous process. During warm periods, enhanced thinning at the grounding line triggers a wave of thinning that propagates inland (Figure 26). Periods of reduced thinning are similarly followed by reduced thinning, or even thickening, inland. For example, the Kohler glacier (Figure 26c) shows a thinning signature initiated pre 1996, however the stability of the current grounding line has prevented any more recent thinning, in contrast to Pine Island and Thwaites glaciers (Figures 26a and 26b).

Using the relationships established in Section 2.3.1 between shelf edge winds (and thus thermocline depth and melt flux) and Pacific SSTs, we can extend our proxy record back in time. Two prominent anomalies occur in the 1940s and 1970s, coinciding with the grounding line events seen in the sediments beneath the Pine Island Glacier. The anomalous period in the 1940s is well documented in ice core records from the West Antarctica, and is the most anomalous period in the 20th century, with the exception of the 1990s.

Records of ice flux across the grounding line of glaciers in the Amundsen region start in the 1970s, when satellite imagery became available. Since the 1970s, each glacier has experienced periods of rapid acceleration and periods of relatively steady flow or slight deceleration. Whilst responses vary from glacier to glacier, it is clear that accelerations correspond with

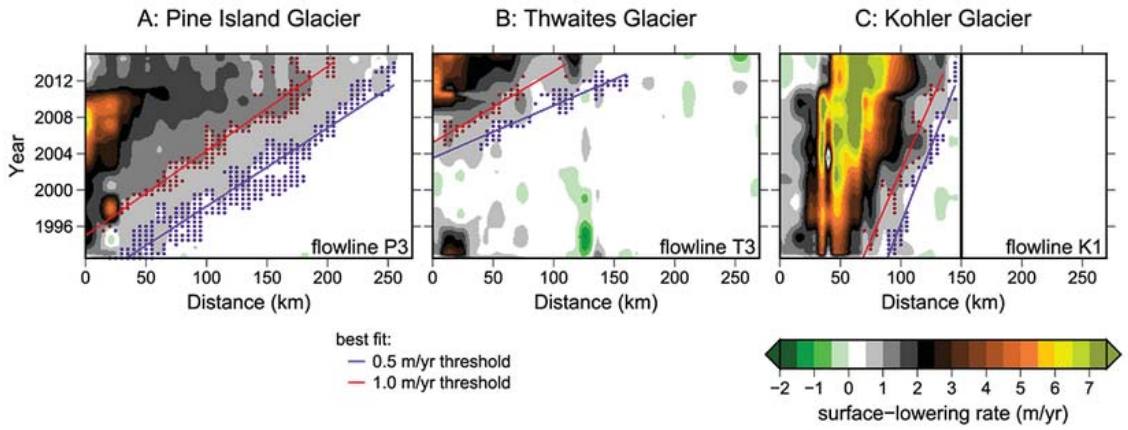

Figure 26: Ice surface-lowering rates along flowlines in the three basins. Figure from [11].

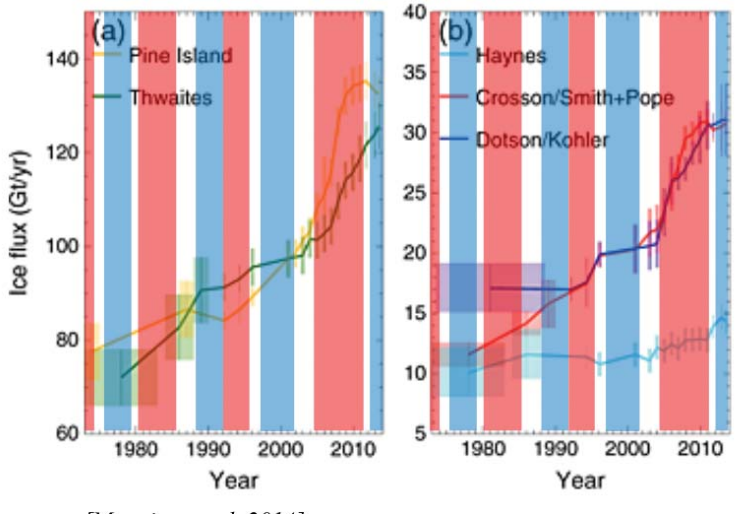

Figure 27: Evolution of ice discharge at the grounding line, where the red shading indicates a warm period and the blue shading is a cool period. Figure adapted from [17].

warm periods, while steady flow coincides with cool periods (Figure 27). The varied responses of individual glaciers is determined by the geometry and properties.

The mechanism for increased melting of an ice shelf driving thinning of a glacier upstream is illustrated in Figure 28. Increased transport of CDW on shelf increases melt rates and thins the glacier (top panel). This decreases the buttressing effect the ice shelf can provide and moves the grounding line back (middle panel), and the glacier accelerates. This changes the surface slope of the glacier, accelerating flow upstream and allowing the thinning signal to propagate. In the lower panel, the ice shelf thickens due to decreased melt, itself a result of a deeper thermocline, which isolates the shelf from CDW.

The propagation of the thinning signal upstream operates on far longer timescales than the adjustment which occurs at the glacier front. Thus, at any one time we may be looking

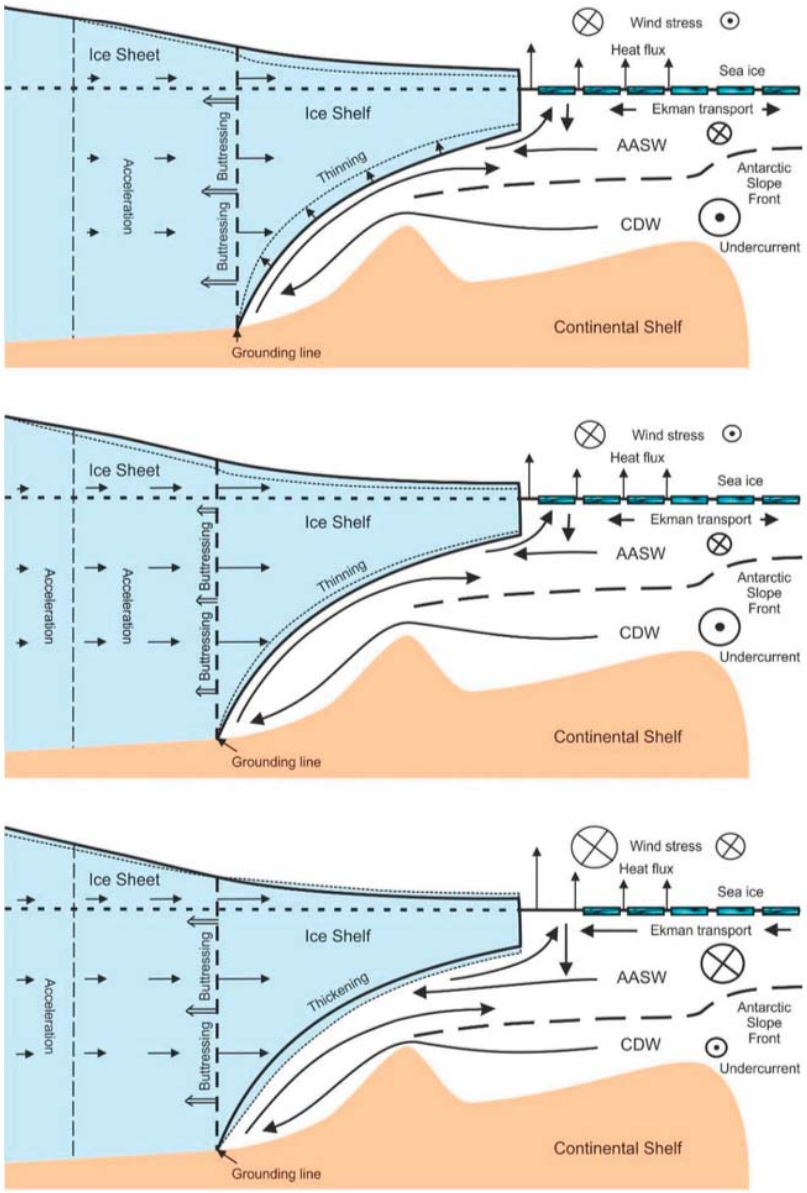

Figure 28: Schematic linking atmospheric and oceanic forcing to ice sheet flow via the thinning/thickening of an ice shelf. *Upper:* CDW accesses the ice shelf cavity, driving high melt. *Middle:* The ice shelf thins and the grounding line retreats. The surface slope increases, as does the grounded ice flow. *Lower:* Increased westerlies lower the thermocline and restrict CDW access, thickening and flattening the ice shelf.

at a superposition of cooling (thickening, advancing) and warming (thinning, retreating) signals. To further complicate the matter, a key factor in the stability of the grounding line is the geometry of the bed, meaning that a given forcing may influence different glaciers in different ways.

2.5 Summary

The Amundsen sea sector is an especially interesting region in that wind variability has the capacity to drive a large response in ice shelves, and consequently in the upstream flow of grounded ice. The sensitivity of the ice to the winds is a result of the ocean state and bathymetry of the region; variability in the thermocline depth and the strength of the slope front undercurrent modulate the on-shelf flow of warm CDW.

Since the 1940s, the ice sheet has been experiencing episodic retreat. Decadal ocean variability can trigger retreat, and once the grounding line is forced from a seabed high, it will continue until the grounding line stabilises long enough for the inland flow to equilibrate. A key question to address is whether, were the shelf to thicken, the previous grounding line could be re-established. In other words, is this a cycle, or is it irreversible?

References

[1] Chavanne, C. P., Heywood, K. J., Nicholls, K. W., and Fer, I. (2010). Observations of the Antarctic slope undercurrent in the southeastern Weddell sea. *Geophysical Research Letters*, 37(13).

[2] Dutrieux, P., De Rydt, J., Jenkins, A., Holland, P. R., Ha, H. K., Lee, S. H., Steig, E. J., Ding, Q., Abrahamsen, E. P., and Schröder, M. (2014). Strong sensitivity of Pine Island ice-shelf melting to climatic variability. *Science*, 343(6167):174–178.

[3] Hattermann, T., Nøst, O. A., Lilly, J. M., and Smedsrud, L. H. (2012). Two years of oceanic observations below the Fimbul Ice Shelf, Antarctica. *Geophysical Research Letters*, 39(12).

[4] Hellmer, H. H., Kauker, F., Timmermann, R., Determann, J., and Rae, J. (2012). Twenty-first-century warming of a large Antarctic ice-shelf cavity by a redirected coastal current. *Nature*, 485(7397):225–228.

[5] Holland, P. R. and Kwok, R. (2012). Wind-driven trends in antarctic sea-ice drift. *Nature Geoscience*, 5(12):872–875.

[6] JacoBS, S., Jenkins, A., Hellmer, H., Giulivi, C., Nitsche, F., Huber, B., and Guerrero, R. (2012). The Amundsen Sea and the Antarctic ice sheet. *Oceanography*, 25(3):154–163.

[7] Jenkins, A. (1999). The impact of melting ice on ocean waters. *Journal of Physical Oceanography*, 29(9):2370–2381.

[8] Jenkins, A., Dutrieux, P., Jacobs, S., Steig, E. J., Gudmundsson, G. H., Smith, J., and Heywood, K. J. (2016a). Decadal ocean forcing and Antarctic ice sheet response: Lessons from the Amundsen Sea. *Oceanography*, 29(4):106–117.

[9] Jenkins, A., Dutrieux, P., Jacobs, S., Steig, E. J., Gudmundsson, G. H., Smith, J., and Heywood, K. J. (2016b). Decadal ocean forcing and Antarctic ice sheet response: Lessons from the Amundsen Sea. *Oceanography*, 29(4):106–117.

[10] Joughin, I. and Padman, L. (2003). Melting and freezing beneath Filchner-Ronne ice shelf, Antarctica. *Geophysical Research Letters*, 30(9). 1477.

[11] Konrad, H., Gilbert, L., Cornford, S. L., Payne, A., Hogg, A., Muir, A., and Shepherd, A. (2017). Uneven onset and pace of ice-dynamical imbalance in the Amundsen Sea Embayment, West Antarctica. *Geophysical Research Letters*, 44(2):910–918.

[12] Larter, R. D., Anderson, J. B., Graham, A. G., Gohl, K., Hillenbrand, C.-D., Jakobsson, M., Johnson, J. S., Kuhn, G., Nitsche, F. O., Smith, J. A., et al. (2014). Reconstruction of changes in the Amundsen Sea and Bellingshausen sea sector of the West Antarctic ice sheet since the last glacial maximum. *Quaternary Science Reviews*, 100:55–86.

[13] Lenaerts, J. T. M., van den Broeke, M. R., van de Berg, W. J., van Meijgaard, E., and Kuipers Munneke, P. (2012). A new, high-resolution surface mass balance map of Antarctica (1979-2010) based on regional atmospheric climate modeling. *Geophysical Research Letters*, 39(4). L04501.

[14] Makinson, K., Holland, P. R., Jenkins, A., Nicholls, K. W., and Holland, D. M. (2011). Influence of tides on melting and freezing beneath Filchner-Ronne Ice Shelf, Antarctica. *Geophysical Research Letters*, 38(6).

[15] Martinson, D. and McKee, D. (2012). Transport of warm Upper Circumpolar Deep Water onto the western Antarctic Peninsula continental shelf. *Ocean Science*, 8(4):433.

[16] Moffat, C., Owens, B., and Beardsley, R. C. (2009). On the characteristics of Circumpolar Deep Water intrusions to the west Antarctic Peninsula continental shelf. *Journal of Geophysical Research: Oceans*, 114(C5).

[17] Mouginot, J., Rignot, E., and Scheuchl, B. (2014). Sustained increase in ice discharge from the Amundsen Sea Embayment, West Antarctica, from 1973 to 2013. *Geophysical Research Letters*, 41(5):1576–1584.

[18] Nicholls, K. W., Østerhus, S., Makinson, K., Gammelsrød, T., and Fahrbach, E. (2009). Ice-ocean processes over the continental shelf of the southern Weddell Sea, Antarctica: A review. *Reviews of Geophysics*, 47(3).

[19] Nøst, O., Biuw, M., Tverberg, V., Lydersen, C., Hattermann, T., Zhou, Q., Smedsrud, L., and Kovacs, K. (2011). Eddy overturning of the Antarctic Slope Front controls glacial melting in the Eastern Weddell Sea. *Journal of Geophysical Research: Oceans*, 116(C11).

[20] Schmidtko, S., Heywood, K. J., Thompson, A. F., and Aoki, S. (2014). Multidecadal warming of Antarctic waters. *Science*, 346(6214):1227–1231.

[21] Smedsrud, L. H., Jenkins, A., Holland, D. M., and Nøst, O. A. (2006). Modeling ocean processes below Fimbulisen, Antarctica. *Journal of Geophysical Research: Oceans*, 111(C1).

[22] Smith, J., Andersen, T. J., Shortt, M., Gaffney, A., Truffer, M., Stanton, T., Bindschadler, R., Dutrieux, P., Jenkins, A., Hillenbrand, C.-D., et al. (2016). Sub-ice-shelf sediments record history of twentieth-century retreat of Pine Island Glacier. *Nature*.

[23] Stewart, A. L. and Thompson, A. F. (2015). Eddy-mediated transport of warm Circumpolar Deep Water across the Antarctic Shelf Break. *Geophysical Research Letters*, 42(2):432–440.

[24] van Lipzig, N. P. M., Turner, J., Colwell, S. R., and van Den Broeke, M. R. (2004). The near-surface wind field over the Antarctic continent. *International Journal of Climatology*, 24(15):1973–1982.

[25] Walker, D. P., Brandon, M. A., Jenkins, A., Allen, J. T., Dowdeswell, J. A., and Evans, J. (2007). Oceanic heat transport onto the Amundsen Sea shelf through a submarine glacial trough. *Geophysical Research Letters*, 34(2).

[26] Walker, D. P., Jenkins, A., Assmann, K. M., Shoosmith, D. R., and Brandon, M. A. (2013). Oceanographic observations at the shelf break of the Amundsen Sea, Antarctica. *Journal of Geophysical Research: Oceans*, 118(6):2906–2918.

GFD 2017 Lecture 8: Testing the Ocean Trigger Hypothesis for Greenland's Recent Glacier Retreat

Fiamma Straneo; notes by Eric Hester and Jessica Kenigson

June 28, 2017

1 Testing the Ocean Trigger Hypothesis for Greenland's Glaciers

1.1 Establishing rates of mass loss in Greenland

The change in mass M of an ice sheet with respect to time is given by

$$\frac{dM}{dt} = SMB - D \tag{1}$$

where SMB represents the surface mass balance and D represents the rate of ice discharge. Here SMB is the difference between the rate of accumulation due to precipitation and the rate of ablation due to surface melt and sublimation, while D represents the rate of loss due to glacial calving and melting at the ice margins by the ocean. In order to accurately monitor and predict the ice sheet mass balance in a changing climate, it is necessary to isolate SMB and D. In Antarctica, mass loss occurs primarily though D (as ambient temperatures are too low to permit significant mass loss from surface melting); in Greenland this is not the case.

Since 2002, GRACE satellite observations of Greenland mass balance changes through gravimetry have provided data on an ice-sheet-wide scale. Figure 1 shows the cumulative mass change of the ice sheet since 2002 as resolved by GRACE. The declining mass is superimposed upon a significant seasonal cycle of SMB.

Prior to GRACE, ice mass changes were necessarily interpolated from scattered in situ observations. Greenland SMB has been relatively adequately monitored since ∼1980. In order to obtain estimates for earlier periods, Greenland Ice Sheet SMB is reconstructed from (typically) atmospheric and snow-pack models. The Regional Atmospheric Climate Model (RACMO) simulates the spatial distribution of climatological SMB from 1958 – 2007 [3]. Spatially, SMB is $\mathcal{O}(1000$ kg m^{-2} yr$^{-1})$ along the coast of southeast Greenland due to significant orographic precipitation. Over much of northern Greenland, SMB is $\mathcal{O}(100$ kg m^{-2} yr$^{-1})$ due to the relatively low precipitation rates in the interior (and by relatively cold temperatures at high latitudes). Over the coastal margin of southwest Greenland, SMB can reach $\mathcal{O}(-1000$ kg m^{-2} yr$^{-1})$, which is attributable to significant surface melting.

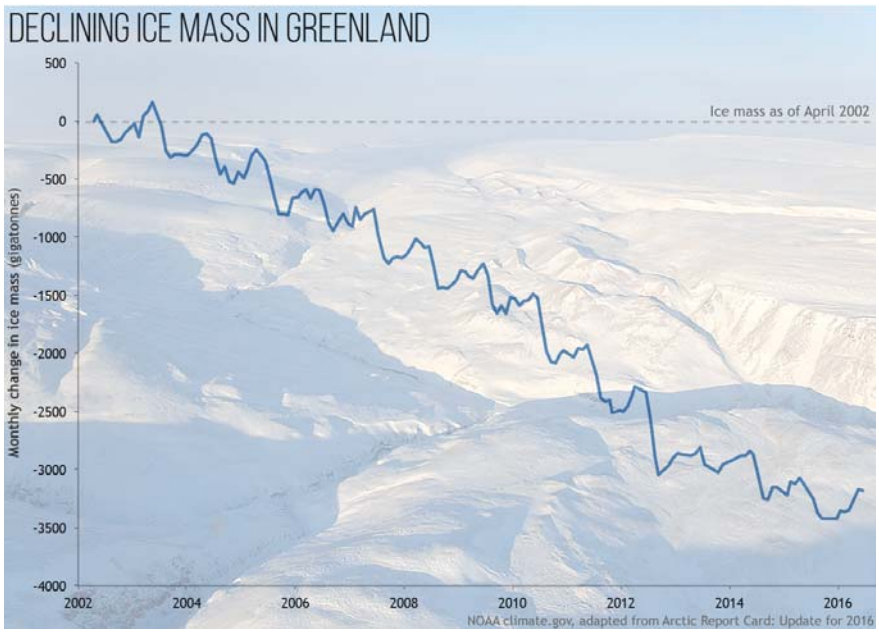

Figure 1: Monthly change in mass of Greenland from April 2002 – April 2016 (cumulative). Figure reproduced from https://www.climate.gov/news-features/featured-images/greenland-ice-mass-loss-continued-2016.

Measurements of D for a particular glacier are made via remote sensing of the ice velocity across a transect (fluxgate) as near as possible to the grounding line, and D is approximated by

$$D = VhH \tag{2}$$

where V is the velocity perpendicular to the transect, h is the width of the fluxgate, and H is the depth of the glacier [5, 2]. Typically, D is assumed to be seasonally invariant (due both to a paucity of observations and, when observations have been available, a lack of evidence of a clear seasonal dependence). In one study, D was calculated at 178 outlet glaciers [2]; V was estimated (where possible) by repeat imaging from the Landsat 7 Enhanced Thematic Mapper Plus and the Advanced Spaceborne Thermal and Reflectance Radiometer (ASTER). In addition, H was obtained from digital elevation models (DEMs) by differencing the bed elevation from the surface elevation (where possible; bed elevation data was not available in the cross-flow direction at all glaciers).

Historical reconstructions of the total mass balance (TMB, defined as $SMB - D$) require estimates of D, which are often based upon correlations between SMB and D over periods in which both quantities have been observed. Figure 2 shows a reconstruction of the Greenland Ice Sheet SMB, D, and TMB from 1900 – 2010 [6]. The historical reconstruction is based upon differences between the maximum extent of the ice sheet during the Little Ice Age (as inferred from trimlines and moraines) and aerial photogrammetry from 1978-1987, which allows the change in elevation around the entire perimeter of the ice sheet to be calculated. This is then interpolated to the interior. SMB modeling is used to resolve the mass balance

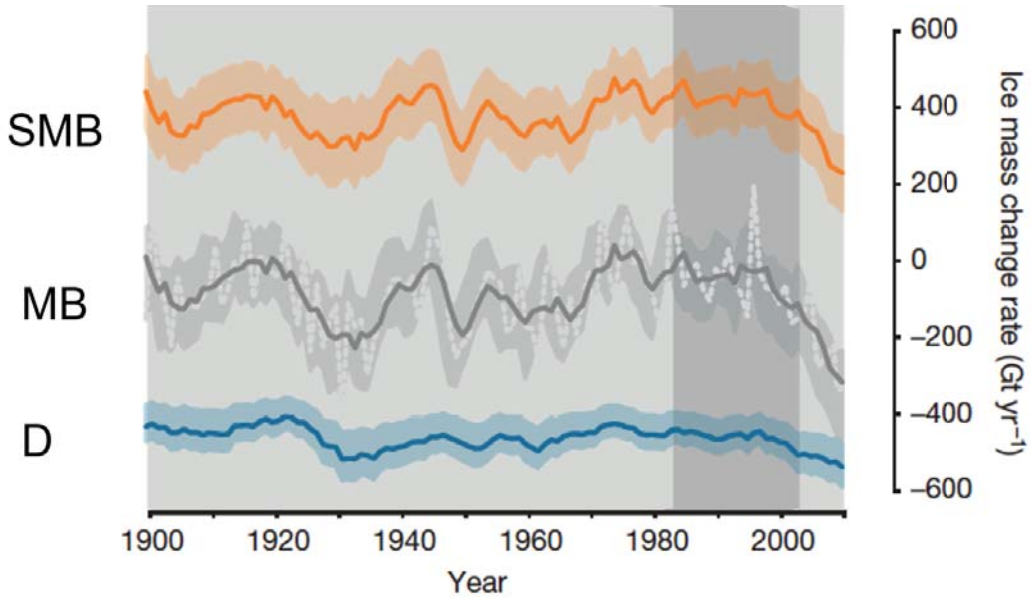

Figure 2: Five-year mean of SMB (orange line), modeled ice discharge (blue line), and 5-year mean of total mass balance (gray) with 1σ uncertainty range (shading). Figure subsetted from [6].

into components arising from SMB and D (see their "Methods" section). Mass loss is seen to significantly accelerate around ∼1990, with mass balance deficits increasing at a rate not seen since perhaps ∼1920⁻1930. What might account for the accelerated mass loss since ∼1990?

1.2 Ocean trigger hypothesis

Changes in both SMB and D contribute in approximately equal part to the mass loss from the Greenland Ice Sheet since ∼1990. Moreover, an accelerated retreat of large outlet glaciers beginning around ∼2000 (primarily around the western and southern coast of Greenland) has been documented.

Two major types of glaciers exist along the margins of Greenland: "floating ice tongue" glaciers and tidewater glaciers. Tidewater glaciers are characterized by a relatively shear vertical face and primarily lose mass through glacial calving, while floating ice tongue glaciers are characterized by a long, thin, floating ice protrusion into the ocean from the grounding line and primarily lose mass through melting. Many of Greenland's large tidewater glaciers (including, for example, Jacobskavn Isbrae, Helheim, and Zachariae Isstrom) had floating ice tongues in the recent past.

The ocean trigger hypothesis [13] suggests that the glacier retreat beginning around ∼2000 (Figure 3) and contributing to the relative increase of D (as in [6]) was initiated by oceanic drivers. The intrusion of anomalously warm ocean water onto the shelf causes submarine melting of the floating ice tongue, triggering rapid thinning and ungrounding, which reduces buttressing and causes acceleration and calving. For instance, Jacobshavn Isbrae transitioned from a regime of slow ice accumulation to rapid thinning beginning around

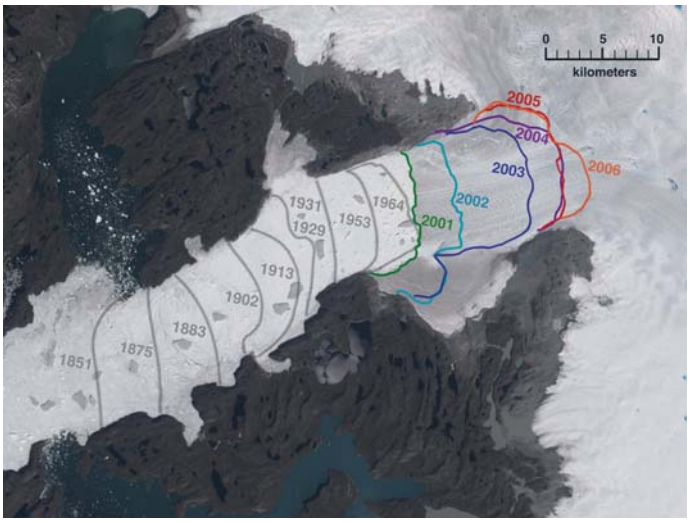

Figure 3: Shift in the calving front at Jacobshavn Isbrae from 1851-2006. Figure reproduced from https://svs.gsfc.nasa.gov/3395.

1997, and this was accompanied by an approximate doubling of velocity [4]. The accelerated mass loss is thought to be associated with warm oceanic inflow from the Irminger Sea. This is in contrast to the hypothesis that atmospheric warming causes enhanced surface melt and bed lubrication, leading to accelerated sliding. Hydrographic data in and around Greenland's fjords is difficult to obtain, particularly at depth. However, this warming signal beginning around 1997 (at depths of 150-600 m) was captured by trawl fishery measurements made from 1991 – 2006.

The ocean trigger hypothesis is supported by several independent lines of evidence. Indeed, ocean currents which bifurcate from the North Atlantic Current transport warm equatorial waters close to the southern coastal shelf of Greenland (Figure 5 shows a schematic diagram), suggesting that it is plausible for outlet glaciers to respond sensitively to changes in ocean temperature. However, few direct measurements of ocean temperature at depth along the shelf are available over the period of interest, requiring the use of sparse direct measurements, proxy data, and models. For instance, a numerical ice-flow model with a dynamic calving front has been used to study the reponse of Helheim glacier to various front-stress perturbations, changes in basal lubrication, and changes in the ablation rate [8]. Experiments with front-stress perturbations (which could occur due to rapid thinning of the floating ice tongue) best captured the observed rate of retreat and lend credence to the ocean trigger hypothesis.

Furthermore, paleooceanographic reconstructions fail to refute the ocean trigger hypothesis. For example, at Disko Bugt (West Greenland), a 100-year long (1910 – 2007) record of ocean temperature at approximately 300 m depth was reconstructed based upon the relative presence of warm and cold water taxa of benthic foraminifera in a series of sediment cores [7]. Indeed, the accelerated retreat of Jacobshavn Isbrae beginning after 1998 coincided with a period of ocean warming locally (and local ocean temperatures were related to the Atlantic Multidecadal Oscillation).

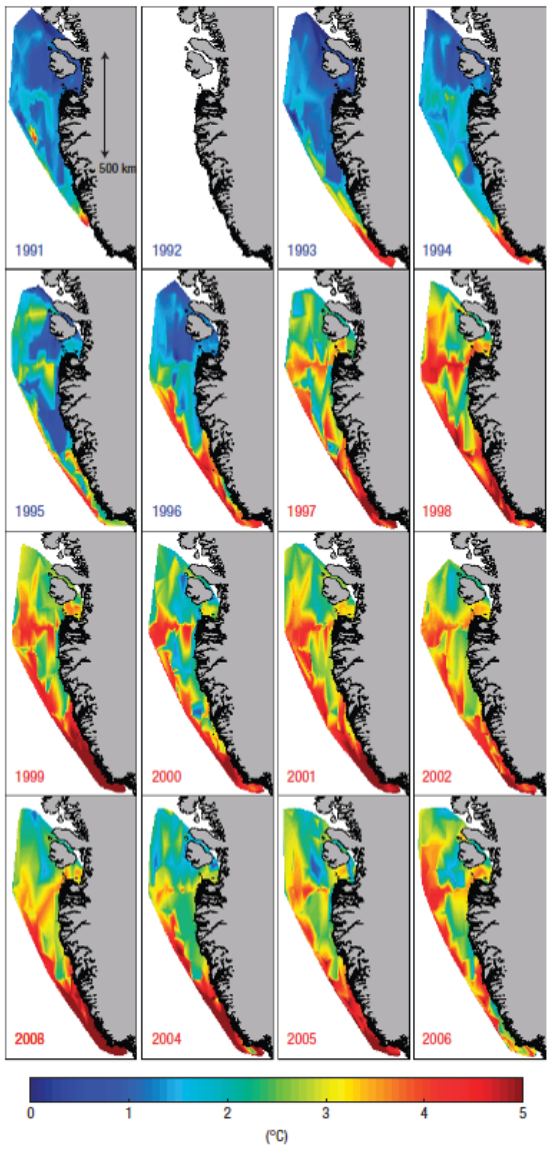

Figure 4: Depth-averaged temperature as obtained from trawl fisheries for1991-2006 (150-600 m average). Note the increase in temperature near Jacobshavn Isbrae in 1997. Figure reproduced from [4].

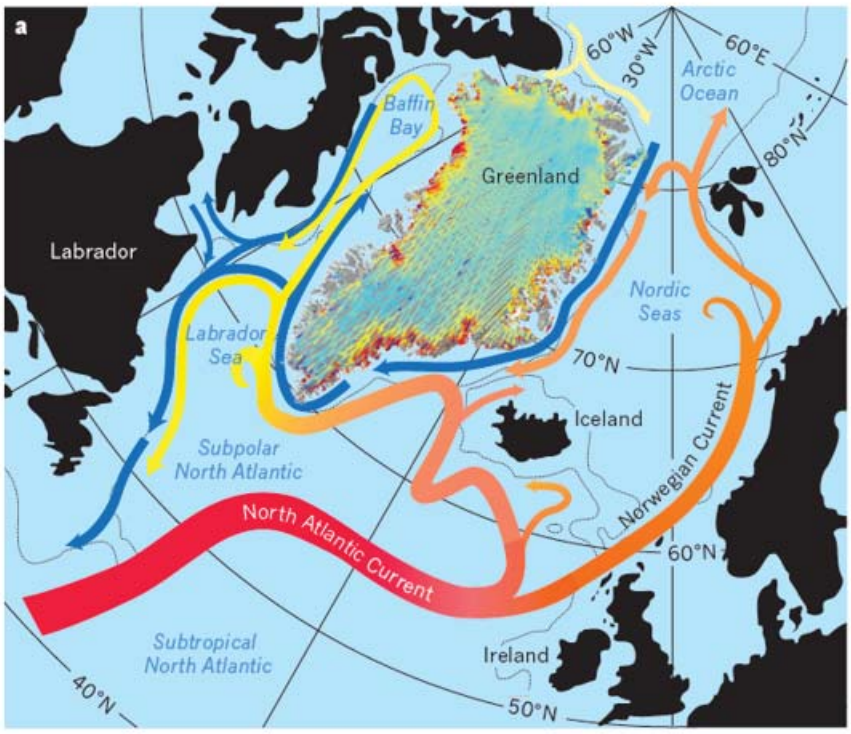

Figure 5: Schematic diagram of the ocean circulation around Greenland. Note the proximity of the warm Irminger Current (warm northward-flowing current branching from the North Atlantic Current to the west) to the coastal shelf of Greenland. Figure adapted from [13].

Calving rates may be reconstructed using the observation that icebergs are "dirty." Specifically, Ice-Rafted Debris (IRD) deposited in Semilik Fjord near the Helheim Glacier terminus has been used as a proxy for glacial calving [1]. Based upon measurements from sediment cores, a record of the calving rate has been reconstructed from 1890 to near present. In particular, the sand fraction is used to represent the IRD since sand grains are likely to have been transported by icebergs rather than advected by meltwater plumes due to their large size (which causes them to rain out of suspension). The authors note that the accelerated calving event of the early 2000s (as well as a period during the early $\sim$1930s – 1940s) was associated with warm phases of the Atlantic Multidecadal Oscillation (indicating that inflowing Atlantic waters were relatively warm) and with relatively low export of cold Arctic water. This supports the hypothesis that enhanced submarine melt at Helheim was triggered by contact with anomalously warm ocean water.

Indeed, the influx of cold Arctic water through the Fram Strait to the coastal margins of Greenland (as indicated by the Storis index, related to the latitude of the sea ice extent along the coast of southwest Greenland) versus the influx of relatively warm water from the south via the North Atlantic Current/Irminger Current (as given by a temperature transect south of Iceland) likely influences the calving rate [1]. For this reason, a "Shelf Index" is constructed as the sum of these indices, and the Shelf Index is seen to correlate with the calving rate on interannual and longer timescales ($r = 0.41$ for 3-year mean, which is statistically significant at the 95% level). Correlations between the (negative) Storis index and Atlantic water temperatures as measured along the transect are nearly as strong, yet correlations with atmospheric variables such as the wintertime North Atlantic Oscillation index are also significant ($r = -0.45$).

Thus, we see that there are multiple independent lines of evidence to support the Ocean Trigger hypothesis.

2 Ice-ocean Interactions in Greenland Glaciers

The evolution of Greenland glaciers depends on a range of complex phenomena, associated with changes in atmospheric and oceanic conditions on multiple spatial and temporal scales.

This lecture will outline the current understanding of the effect of oceanic forcing on Greenland glaciers, and the techniques used to establish these facts.

2.1 Greenland glaciers: tidewater vs tongues

There are two types of outlet glaciers in Greenland, characterised by their structure beyond their grounding line (the furthest point at which they are in contact with the sea bed).

The first and most common, tidewater glaciers, do not extend far beyond their grounding line, and display vigorous calving (iceberg production) at their edge. The other type, floating tongue glaciers, instead extend tens of kilometres beyond their grounding line. Further, floating ice tongues typically balance the incoming ice flux by melt, and do not strongly calve. Floating tongue glaciers are able to balance the incoming ice flux by melt as they have a much larger area in contact with the fjord waters.

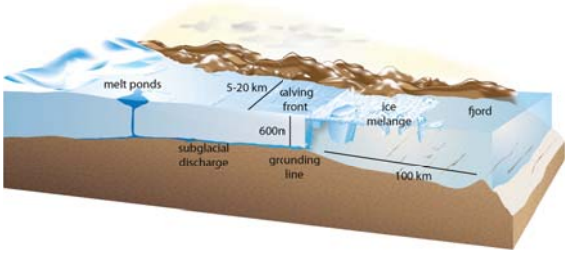

Figure 6: Schematic of typical Greenland tidewater glacier. Figure adapted from [14].

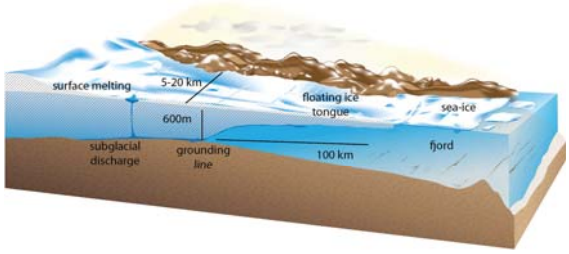

Figure 7: Floating tongue glaciers extend far beyond the grounding line. Figure adapted from [14].

2.2 Ocean water in fjords

The waters surrounding East Greenland are divided between two dominant water types – the warmer Atlantic water (AW) supplied by the North Atlantic current, and cooler polar water (PW) from the pole (Figure 8). The location of these waters, and in particular their interaction with glaciers when within the fjord, is believed to control glacial melting.

Straneo et. al. [12] performed ship and mooring based measurements of oceanographic data in Sermilik Fjord during 2008. They found the bottom of the fjord (beyond 200-300 m) was filled with warmer Atlantic water, while cooler polar water resided in the higher layers. These two modes were supplemented by a third water mass of glacial meltwater during the summer.

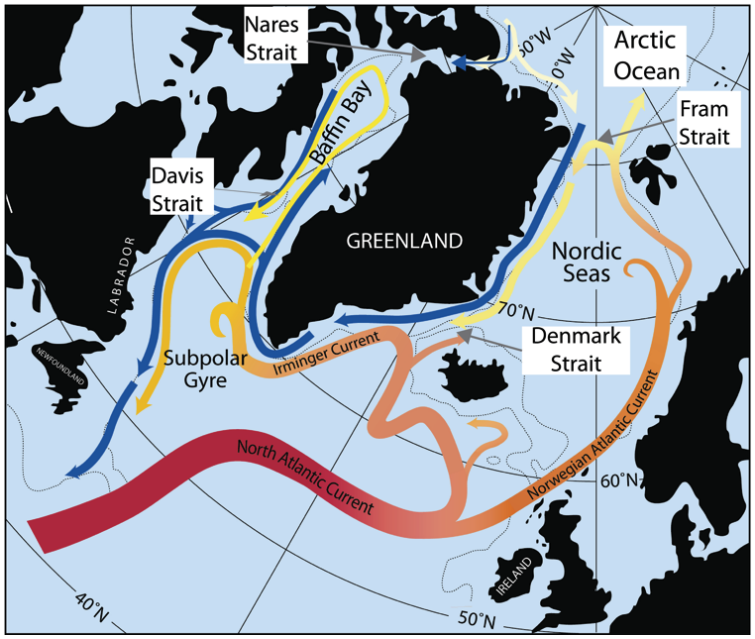

Figure 8: Schematic of ocean currents around Greenland. Figure from [10].

Importantly, they found that these waters were continuously replenished [12]. There are several mechanisms that contribute to this replacement, but one main driver of fjord/shelf

exchange is variations in the pycnocline on the shelf near the mouth of the fjord.

Figure 9 illustrates this mechanism with the example of Ekman transport by along coast winds. These winds (into the page) force transport of the surface layer toward the right (into the fjord), depressing the shelf pycnocline. The fjord waters then equilibrate to this new stratification by inflow of the top polar water, and outflow of the bottom Atlantic water. When the forcing ceases, the fjord waters will then relax to the original equilibrium, thereby replenishing the waters.

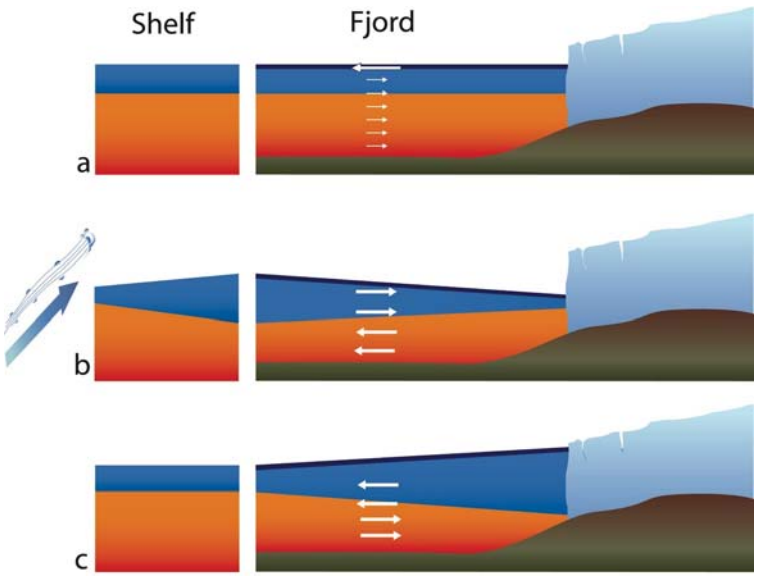

Figure 9: Wind driven forcing of shelf waters will adjust the shelf pycnocline, to which the fjord waters equilibrate. When the forcing ceases, the fjord waters readjust to the previous equilibrium (c). Figure adapted from [12] (Supplementary Information).

The presence of high sills in fjords may be able to block this transfer however [9, 16], mitigating the i nfluence of the warmer Atlantic water.

2.3 Glacial melt from temperature-salinity diagrams

The distribution of fjord water characteristics is highly revealing when plotted on a (potential) Temperature (θ) - Salinity (S) diagram. This is because when salt water melts ice, the properties of the water-ice mixture will evolve along a straight line in $\theta - S$ space - as explained in Adrian Jenkins' first lecture. Water measurements close to the line imply the melting of glacial ice; divergence implies some other process is occurring (such as mixing with glacial runoff).

Straneo and others [11, 15] found that measurements around Greenland glaciers were consistent with melting of glaciers by Atlantic Water. The red curves in Figure 10 show $\theta - S$ measurements of water near the fjord mouth, while the blue curves are near the glacier. The winter measurements (on the right), show that water near the glacier lies closer to the melting line of Atlantic water, implying that the water is melting the glacier.

The summer measurements tell a different story however. Now, the near-glacier water diverges from the melting line of the Atlantic water, instead being much fresher than expected. This is due to discharge, including at depth, of surface melt driven by a warm atmosphere above the ice.

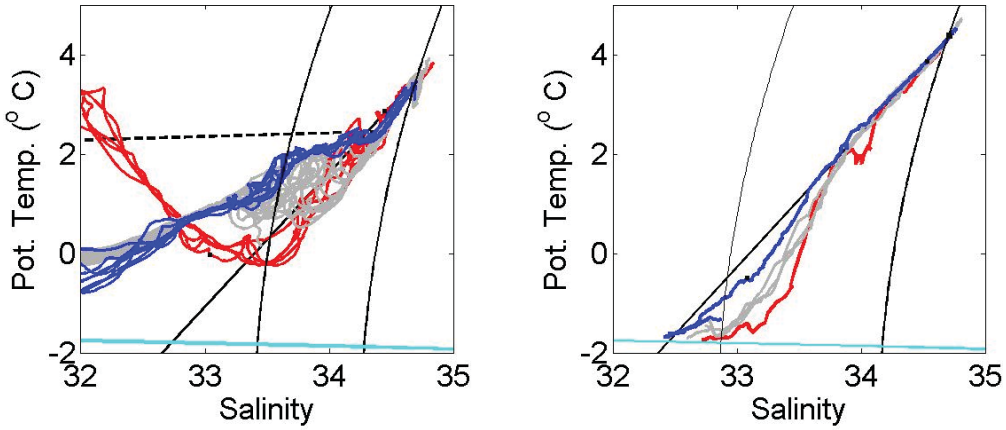

Figure 10: $\theta - S$ measurements near Helheim glacier in summer (left) and winter (right). The red curves are of waters near the mouth of the fjord, and the blue readings are as close as possible to the glacier edge. The influence of the glacier is seen through the differences between the red and blue curves. The solid black line shows the melting line of Atlantic water, while the dashed line shows the line for mixing with glacial runoff. The curved lines are isopycnals, the cyan line shows the freezing temperature at zero pressure for varying salinities. Figure adapted from [11].

2.4 Lagrangian ice flux divergence measurements

The melting of ice tongues can be inferred by measuring the divergence of the ice flow. Assuming a vertically uniform velocity $\boldsymbol{u} = (u, v)$ and density ρ_i, the melt rate $\dot{a}$ of a floating ice tongue can be inferred from the conservation law for ice thickness h:

$$\frac{\partial h}{\partial t} + \nabla \cdot (h\boldsymbol{u}) = \frac{\partial h}{\partial t} + \boldsymbol{u} \cdot \nabla h + h \nabla \cdot \boldsymbol{u} = \dot{a}. \tag{3}$$

This Eulerian framework suffers from a key drawback however; for sparse sampling times, the calculation of time derivatives will be affected by *aliasing* – If the sampling time is too sparse and a second peak is in the same location as a past peak, then there is no way to infer a change in thickness of the ice.

A more effective approach is to switch to a Lagrangian framework, in which we track the time derivative of the ice thickness *following the ice*, $Dh/Dt = \partial h/\partial t + \boldsymbol{u} \cdot \nabla h$. By tracking the ice, we are able to minimize aliasing. This gives our conservation law as

$$\frac{Dh}{Dt} + h \nabla \cdot \boldsymbol{u} = \dot{a}. \tag{4}$$

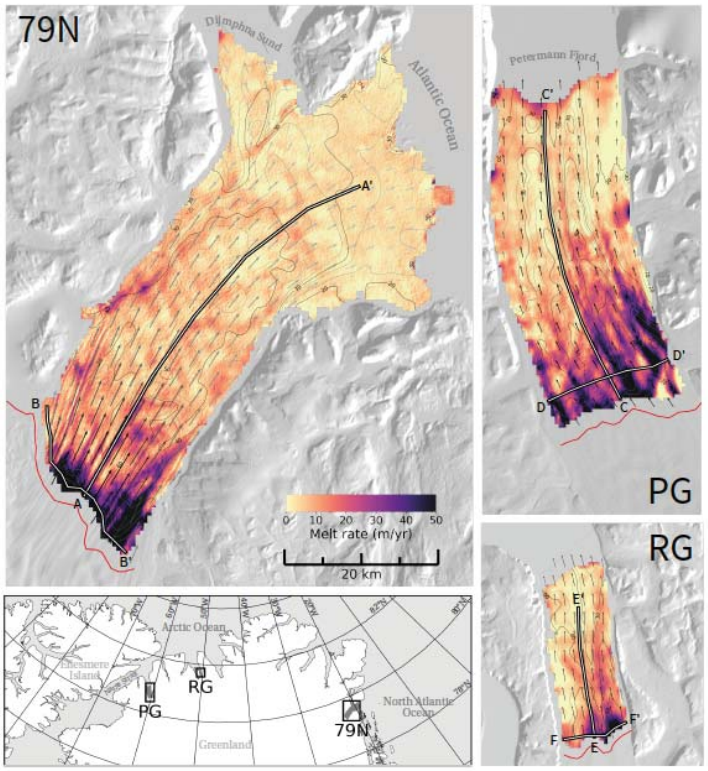

Figure 11: Greenland glacier melt rates determined using Lagrangian ice flux divergence measurements. Figure from [17].

The first step in estimating these quantities is to measure the surface elevation of the ice tongue using Digital Elevation Maps at multiple times.

The thickness of the ice tongue can the be measured given knowledge of the tidal data, and assuming hydrostatic balance of the ice. The hydrostatic approximation becomes invalid within several kilometres of the grounding line, preventing the use of this technique in these areas.

By cross correlating successive elevation maps, the velocity of the ice $\boldsymbol{u}$ can be inferred, and the elevation (thus thickness) change Dh/Dt can be measured. From these measurements, the total melt rate of the ice tongue can then be inferred. The submarine melting can finally be isolated by subtracting the surface melt using a model of atmospheric melting. Putting all this together, the subglacial melt of glaciers can be calculated, as seen in Figure 11 for three Greenland glaciers [17].

References

[1] C. S. Andresen, F. Straneo, M. H. Ribergaard, A. A. Bjørk, T. J. Andersen, A. Kuijpers, N. Nørgaard-Pedersen, K. H. Kjær, F. Schjøth,

K. Weckström, et al., *Rapid response of Helheim Glacier in Greenland to climate variability over the past century*, Nature Geoscience, 5 (2012), pp. 37–41.

[2] E. M. Enderlin, I. M. Howat, S. Jeong, M.-J. Noh, J. H. Angelen, and M. R. Broeke, *An improved mass budget for the Greenland ice sheet*, Geophysical Research Letters, 41 (2014), pp. 866–872.

[3] J. Ettema, M. R. van den Broeke, E. van Meijgaard, W. J. van de Berg, J. L. Bamber, J. E. Box, and R. C. Bales, *Higher surface mass balance of the Greenland ice sheet revealed by high-resolution climate modeling*, Geophysical Research Letters, 36 (2009).

[4] D. M. Holland, R. H. Thomas, B. De Young, M. H. Ribergaard, and B. Lyberth, *Acceleration of Jakobshavn Isbrae triggered by warm subsurface ocean waters*, Nature geoscience, 1 (2008), pp. 659–664.

[5] I. M. Howat, I. Joughin, and T. A. Scambos, *Rapid changes in ice discharge from Greenland outlet glaciers*, Science, 315 (2007), pp. 1559–1561.

[6] K. K. Kjeldsen, N. J. Korsgaard, A. A. Bjørk, S. A. Khan, S. Funder, N. K. Larsen, J. L. Bamber, W. Colgan, M. van den Broeke, M.-L. Siggaard-Andersen, et al., *Spatial and temporal distribution of mass loss from the Greenland Ice Sheet since AD 1900*, Nature, 528 (2015), pp. 396–400.

[7] J. Lloyd, M. Moros, K. Perner, R. J. Telford, A. Kuijpers, E. Jansen, and D. McCarthy, *A 100 yr record of ocean temperature control on the stability of Jakobshavn Isbrae, West Greenland*, Geology, 39 (2011), pp. 867–870.

[8] F. M. Nick, A. Vieli, I. M. Howat, and I. Joughin, *Large-scale changes in Greenland outlet glacier dynamics triggered at the terminus*, Nature Geoscience, 2 (2009), pp. 110–114.

[9] F. Schjoth, C. S. Andresenb, F. Straneo, T. Murray, K. Scharrer, and A. Korablev, *Campaign to map the bathymetry of a major Greenland fjord*, Eos, Transactions American Geophysical Union, 93 (2012), pp. 141–142.

[10] F. Straneo and C. Cenedese, *The dynamics of Greenland's glacial fjords and their role in climate*, Annual Review of Marine Science, 7 (2015), pp. 89–112. PMID: 25149564.

[11] F. Straneo, R. G. Curry, D. A. Sutherland, G. S. Hamilton, C. Cenedese, K. Vage, and L. A. Stearns, *Impact of fjord dynamics and glacial runoff on the circulation near Helheim Glacier*, Nature Geosci, 4 (2011), pp. 322–327.

[12] F. Straneo, G. S. Hamilton, D. A. Sutherland, L. A. Stearns, F. Davidson, M. O. Hammill, G. B. Stenson, and A. Rosing-Asvid, *Rapid circulation of warm subtropical waters in a major glacial fjord in East Greenland*, Nature Geosci, 3 (2010), pp. 182–186.

[13] F. Straneo and P. Heimbach, *North Atlantic warming and the retreat of Greenland's outlet glaciers*, Nature, 504 (2013), pp. 36–43.

[14] F. Straneo, P. Heimbach, O. Sergienko, G. Hamilton, G. Catania, S. Griffies, R. Hallberg, A. Jenkins, I. Joughin, R. Motyka, W. T. Pfeffer, S. F. Price, E. Rignot, T. Scambos, M. Truffer, and A. Vieli, *Challenges to understanding the dynamic response of Greenland's marine terminating glaciers to oceanic and atmospheric forcing*, Bulletin of the American Meteorological Society, 94 (2013), pp. 1131–1144.

[15] F. Straneo, D. Sutherland, D. Holland, C. Gladish, G. Hamilton, H. Johnson, E. Rignot, Y. Xu, and M. Koppes, *Characteristics of ocean waters reaching Greenland's glaciers*, Annals of Glaciology, 53 (2012), pp. 202–210.

[16] D. A. Sutherland, F. Straneo, G. B. Stenson, F. J. Davidson, M. O. Hammill, and A. Rosing-Asvid, *Atlantic water variability on the SE Greenland continental shelf and its relationship to sst and bathymetry*, Journal of Geophysical Research: Oceans, 118 (2013), pp. 847–855.

[17] N. Wilson, F. Straneo, and P. Heimbach, *Submarine melt rates and mass balance for Greenland's remaining ice tongues*, The Cryosphere, 2017 (in press, 2017), pp. 1–17.